JCI The Journal of Clinical Investigation

Inhibition of relaxin autocrine signaling confers therapeutic vulnerability in ovarian cancer

Helen E. Burston, … , Anne-Marie Mes-Masson, Robert Rottapel

J Clin Invest. 2021. https://doi.org/10.1172/JCI142677.

Research In-Press Preview **Oncology**

Graphical abstract

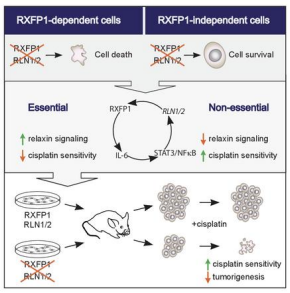

Inhibition of relaxin autocrine signaling confers therapeutic vulnerability in ovarian cancer

Authors: Helen E. Burston[1], Oliver A. Kent[1], Laudine Communal[2], Molly L. Udaskin[1], Ren X. Sun[1], Kevin R. Brown[3], Euihye Jung[4], Kyle E. Francis[1], Jose La Rose[1], Joshua Lowitz[5], Ronny Drapkin[4], Anne-Marie Mes-Masson[2,6] and Robert Rottapel[1,7*]

Affiliations:

1. Princess Margaret Cancer Centre, University Health Network, Toronto, ON, Canada.
2. Centre de recherche du Centre hospitalier de l'Université de Montréal (CRCHUM), Montreal, QC, Canada; Institut du Cancer de Montréal, Montréal, QC, Canada.
3. Banting and Best Department of Medical Research, Donnelly Centre for Cellular and Biomolecular Research, University of Toronto, Toronto, ON, Canada.
4. Penn Ovarian Cancer Research Center, University of Pennsylvania, Philadelphia, PA, USA.
5. Antibody Solutions, Santa Clara, CA, USA.
6. Département de Médecine, Université de Montréal, Montreal, QC, Canada.
7. Department of Medical Biophysics, Department of Immunology, University of Toronto, Toronto, ON, Canada; Division of Rheumatology, St. Michael's Hospital, Toronto, ON, Canada.

Correspondence:

Robert Rottapel

Princess Margaret Cancer Centre, 101 College Street TMDT 12-701, Toronto ON M5G 1L7

rottapel@gmail.com (416)-581-7852

Running title: Relaxin Signaling in OC.

Conflict of interest statement: The authors have declared that no conflict of interest exists.

ABSTRACT

Ovarian cancer (OC) is the most deadly gynaecological malignancy with unmet clinical need for new therapeutic approaches. The relaxin peptide is a pleiotropic hormone with reproductive functions in the ovary. Relaxin induces cell growth in several types of cancer, but the role of relaxin in OC is poorly understood. Here, using cell lines and xenograft models, we demonstrated that relaxin and its associated G-protein coupled receptor RXFP1 form an autocrine signaling loop essential for OC in vivo tumorigenesis, cell proliferation and viability. We determined that relaxin signaling activated expression of pro-oncogenic pathways including RHO, MAPK, Wnt and Notch. We found that relaxin is detectable in patient derived OC tumors, ascites and serum. Further, inflammatory cytokines IL-6 and TNF-α activated transcription of relaxin via recruitment of STAT3 and NFκB to the proximal promoter initiating an autocrine feedback loop that potentiated expression. Inhibition of *RXFP1* or relaxin increased cisplatin sensitivity of OC cell lines and abrogated in vivo tumor formation. Finally, we demonstrated that a relaxin neutralizing antibody reduced OC cell viability and sensitized cells to cisplatin. Collectively, these data identified the relaxin-RXFP1 autocrine loop as a therapeutic vulnerability in OC.

INTRODUCTION

Ovarian cancer has the highest mortality rate of all gynecological malignancies. High-grade serous ovarian carcinoma (HGSOC) is the most common and aggressive subtype with a dismal 5-year survival rate of 30% (1). Poor survival has been linked to early asymptomatic metastatic progression accompanied by dissemination of cancer cells throughout the peritoneal cavity (2). The standard treatment for HGSOC is cytoreductive surgery followed by platinum-based chemotherapy. Although most women initially respond to chemotherapy, the majority of patients will suffer disease recurrence following treatment and 70% will die of recurrent disease within 5 years of initial diagnosis (3). There is an urgent unmet need to identify new targets that can be drugged therapeutically. Targeted therapies may demonstrate greater selectivity, lower toxicity, and improved outcome over conventional chemotherapy (4).

G-protein-coupled receptors (GPCRs) and their ligands underlie several aspects of cancer initiation and progression, including aberrant cell proliferation, metastasis, adhesion and angiogenesis (5). GPCR-ligand interactions are highly druggable, which makes them attractive for cancer drug-discovery research (6). The GPCR encoding the relaxin receptor (RXFP1) and its ligand relaxin regulate pleiotropic functions across a variety of tissues (7). Relaxin family peptides are part of the insulin superfamily and include both relaxin and insulin-like (INSL) peptides. Relaxin plays a central role in reproduction and mediates follicle growth, endometrial differentiation and uterine angiogenesis prior to implantation. The ovaries and prostate are the two major sources of relaxin in humans. Relaxin-2 (*RLN2*) and the highly similar *RLN1* are co-expressed at low levels in multiple tissues including the decidua, placenta, endometrium, prostate, and myocardium and act both as autocrine and paracrine hormones (8). Relaxin peptides are processed from a propeptide form (pro-RLN) to produce mature peptides containing an A-chain linked to a B-chain by two disulphide bonds (7). Upon activation, RXFP1 couples to the small g-proteins $G\alpha_s$ and $G\alpha_{i3}$ to initiate production of adenosine 3',5'-monophosphate (cAMP) as well as activation of phosphoinositide 3-kinase (PI3K) and the RAF-MEK-ERK (MAPK) signaling pathways (7,9). There is increasing evidence that relaxin may play a central role in multiple cancers, particularly cancers of reproductive origin (10).

Here, we identified relaxin-RXFP1 as an essential autocrine loop in a subset of OC cell lines. We explored the role of the relaxin-RXFP1 signaling pathway in the initiation and progression of ovarian tumorigenesis, its activation by inflammatory mediators and contribution to platinum resistance and developed an antibody-based reagent targeting RLN2 with therapeutic potential.

RESULTS

The GPCR RXFP1 is essential for survival in a subset of OC cells.

To identify GPCRs that support the survival of ovarian cancer (OC) cells, a genome-wide screening in 33 epithelial OC cell lines: 28 HGSOC, 1 clear cell, and 4 of unknown histotype based on the suitability scores described by Domcke et al., Beaufort et al. and Medrano et al. was performed (Supplementary Figure S1A) (11–14). Twenty-two of the cell lines were derived from individual patients, and the remaining were isogenic pairs derived from one of these 22 lines (11). Each receptor was ranked based on the frequency of essentiality across cell lines (zGARP-associated p-value $p<0.05$). The screen contained shRNAs targeting 376 GPCRs and revealed the relaxin receptor *RXFP1* as the most frequently essential GPCR, with 19 lines demonstrating dependency (Figure 1A , Supplementary Figure S1A). There are four relaxin-related receptor genes in the human genome. RXFP1 and RXFP2 share 60% amino acid sequence homology, while RXFP3 and RXFP4 are considerably more divergent (15). *RXFP2* was essential in 6 cell lines, 3 of which are also dependent on *RXFP1* (Supplementary Figure S1A).

RXFP1 expression was assessed in OC organoids established from 2 patients with HGSOC (OC-organoid 1 and OC-organoid 2). Both stained positively for PAX8, which is expressed in 80-96% of HGSOCs (16). OC-organoid 1 showed a loss of *TP53* expression, while OC-organoid 2 demonstrated strong positive staining, indicative of a stabilizing *TP53* mutation (Figure 1B). Both organoids stained positively for RXFP1, confirming expression in this HGSOC model system. RXFP1 expression was detected in squamous epithelial cells (Supplementary Figure S1C) consistent with the reported staining for the Human Protein Atlas (HPA) approved antibody (17).

To validate essentiality of *RXFP1* in secondary screens, eight OC cell lines were selected demonstrating a range of *RFXP1* expression and dependency (Supplementary Figure S1A and S1B). The cell line panel included OVCAR8, SKOV3, PEO4, PEO6, OAW42, PEA1, PEA2, and OVCAR5. Each was infected with two independent shRNAs (sh1-*RXFP1* or sh2-*RXFP1*) targeting *RXFP1*, a non-targeting control shRNA (shGFP), or shRNA targeting the essential gene *PSMD1* (sh-*PSMD1*). Knockdown of *RXFP1* potently impaired proliferation of OVCAR8, SKOV3, PEO4, and PEO6, whereas OAW42 and PEA2 demonstrated intermediate dependency (Figure 1C, Supplementary Figures S1D and S1E). PEA1 and OVCAR5, which do not express detectable levels of *RXFP1* were resistant to knockdown. Interestingly, OVCAR8 carry missense mutations in both *RXFP2 (*L737F) and *RXFP3* (T76P) *(broadinstitute.org/ccle)*. RXFP2-L737F is contained within the N-terminal cytosolic region, which forms the docking site for $G\alpha_{i3}$, while RXFP3-T76P is contained within the receptor ligand binding/extracellular domain. As we were unable to detect expression of *RXFP2,* the effects of *RXFP2* knockdown could not be evaluated. Both

OVCAR8 and SKOV3 express significantly higher levels of $G\alpha_{i3}$ relative to other cell lines *(BioGPS Cell Line Gene Expression Profiles*), suggesting that *RXFP1* dependency could arise from expression and function of RXFP1 and related receptors, as well as downstream signaling components.

OVCAR8 and SKOV3 depleted of *RXFP1* demonstrated a rounded morphology suggestive of apoptosis activation (Figure 1D). Consistent with this phenotype, increased PARP and caspase-3 cleavage, decreased expression of the anti-apoptotic protein BCL2 and increased propidium iodide (PI) annexin-V staining, confirming apoptosis was observed (Figure 1E, Supplementary Figure S1F). OVCAR5 showed no change in PI annexin-V staining following *RXFP1* knockdown (Supplementary Figure S1F). *RXFP1* is therefore required for survival in a subset of OC cell lines.

***RXFP1* is essential for tumorigenesis of OC cells.**

The contribution of *RXFP1* to tumorigenic phenotypes in OC cells was next examined. Knockdown of *RXFP1* decreased anchorage independent growth of OVCAR8 and SKOV3 but had no effect on OVCAR5 (Figure 1F, Supplementary Figure S1G). *RXFP1* knockdown in OVCAR8 impaired tumor formation when injected into the mammary fat pad of NOD/SCID/IL2R$\gamma^{-/-}$ (NSG) mice compared to shGFP control (Supplementary Figures S1I to S1L).

To determine if *RXFP1* was essential for sustained tumor growth, OVCAR8 were engineered to express a tetracycline (TET)-inducible shRNA targeting *RXFP1* (TET-sh1-*RXFP1*) or control shGFP (TET-shGFP). Induction of shRNA expression with Doxycycline (Dox) resulted in knockdown of *RXFP1* mRNA with a concomitant decrease in cell viability compared to OVCAR8 grown in the absence of Dox (Figure 1G and Supplementary Figure S1M). In the absence of Dox, OVCAR8-derived tumors containing TET-shGFP or TET-sh1-*RXFP1* demonstrated robust growth (Figures 1H to 1J). In contrast, mice given Dox from onset (Dox D0) demonstrated a significant reduction in tumor growth relative to control groups. Mice given Dox 21 days post injection (2 weeks following the appearance of measurable tumors) demonstrated a reduction in tumor growth with final tumor volumes ~50% smaller than tumors in control groups (Figures 1H to 1J). Thus, *RXFP1* contributed to both OC tumor initiation and progression in xenograft models.

Relaxin activates proliferative signaling pathways via RXFP1.

Given the deleterious effect of *RXFP1* knockdown, the effect of relaxin on OC cells was examined. Recombinant human relaxin (rhRLN2) induced increased viability in OVCAR8 and SKOV3 (Figure 2A). Relaxin stimulation increased BrdU incorporation and activated MAPK and AKT signaling in OVCAR8, which was blocked in cells with *RXFP1* knockdown, corroborating that relaxin-induced signaling

is dependent upon *RXFP1* expression. (Figures 2B and 2C, Supplementary Figure S2A). Relaxin stimulation promoted five-fold increased cAMP production in OVCAR8 (Supplementary Figure S2B).

To discover the transcriptional program induced by relaxin, RNA sequencing was performed in OVCAR8 treated with rhRLN2. In total, 766 mRNAs were upregulated and 73 mRNAs downregulated in response to rhRLN2 treatment. Among the upregulated mRNAs were known relaxin target genes including *VEGF* and matrix metalloproteases (*MMPs)* (18, 19). Enrichment analysis revealed gene signatures including RHO GTPase signaling, extracellular matrix regulation, cell adhesion, actin cytoskeleton, and signaling via MAPK, WNT, and NOTCH (Figure 2D). Relaxin-induced target genes involved in tissue remodelling and angiogenesis (*VEGFA*, *MMP9, MMP23*), Notch signaling (*NOTCH1*, *NOTCH3*), transcription (*FOXL2, SOX12, ARID5A*) and WNT signaling (*DVL1, BCL9, LRP5*) were validated (Figure 2E, Supplementary Figure S2C). CRISPR dropout screens revealed that OVCAR8 and SKOV3 shared common genetic dependencies on relaxin induced genes (Supplementary Figure S2D) (20–22). Amplification of relaxin-regulated genes was found in a large percentage (5-18% per gene) of HGSOC tumors in the TCGA dataset (Supplementary S2E) (23–25). Relaxin signaling therefore results in the activation of multiple pathways supporting tumorigenesis.

Relaxin autocrine signaling promotes survival in OC cells.

The human genome contains two relaxin genes, relaxin-1 (*RLN1*) and relaxin-2 (*RLN2*) expressed from *RLN1* and *RLN2* respectively, which share 84% protein sequence identity and both activate RXFP1 (26). For clarity, we refer to the human relaxin peptides/protein collectively as relaxin and genes as RLN. There is reported crosstalk between relaxin-related ligands and receptors (Figure 3A). In addition to RXFP1, relaxin can also interact with RXFP2, although with weaker affinity (27). INSL3 is specific for RXFP2. The highly divergent relaxin-3 (*RLN3*), the cognate ligand for RXFP3, is also capable of RXFP1 activation but is expressed predominantly in the brain (28).

RNA-Seq analysis revealed that *RLN1* and *RLN2* were co-expressed in OC cell lines at low but detectable levels, with *RLN2* generally exhibiting higher expression relative to *RLN1* (Supplementary Figure S3A). *RLN*3 expression was undetectable (FPKM=0) in the majority of lines. OVCAR8 and SKOV3 express predominantly *RLN1* while PEA2 primarily express *RLN2* (Figure 3B). Expression of *RLN* in OC cells correlated with dependency on *RXFP1*. To determine if OC cells exhibited relaxin dependency, *RLN1* and *RLN2* were knocked down using two independent shRNAs (sh1-RLN and sh2-RLN) that target sequences common to both *RLN1* and *RLN2* (Supplementary Figure S3B) and confirmed to knockdown *RLN1* in OVCAR8 and SKOV3, and *RLN2* in PEA2 (Supplementary Figures S3C to S3E). OVCAR5

demonstrated decreased expression of both *RLN1* and *RLN2* in cells expressing sh1-RLN and sh2-RLN (Supplementary Figures S3C and S3D). Relaxin was detectable in supernatants collected from OVCAR8, SKOV3, PEA2, and OVCAR5, but reduced in cells expressing sh1-RLN and sh2-RLN confirming the specificity of the shRNA (Figure 3C, Supplementary Figures S3E and S3F). Knockdown of RLN increased cleavage of PARP and CASP3 and decreased levels of BCL2 in OVCAR8 and SKOV3 compared to shGFP control (Figure 3D).

Knockdown of RLN phenocopied knockdown of *RXFP1* in the panel of cell lines tested (Figure 3E), with OVCAR8 and SKOV3 being the most dependent and OVCAR5 the least dependent. Consistent with dependency of the ligand-receptor pair, RLN knockdown abrogated colony formation in OVCAR8 and SKOV3 but not in OVCAR5 (Figure 3F, Supplementary Figure S3G)

OVCAR8 expressing sh1-RLN had a delayed onset of tumorigenesis with tumors being undetectable until 3 weeks post injection (Figures 3G and 3H). In contrast, OVCAR8 expressing shGFP formed measurable tumors in NSG mice 1.5 weeks post injection. Tumors established from OVCAR8 - shGFP reached a final volume of 550 mm^3 whereas tumors from OVCAR8-sh1-RLN were 45% smaller and reached an average volume of 300mm^3 (Figures 3G and 3H, Supplementary Figure S3H). Positive CD31 staining, a marker of microvasculature (29) was observed in shGFP control tumors and significantly decreased in tumors expressing shRLN (Figures 3I and 3J, Supplementary Figure 3I). Therefore, relaxin is required for optimal growth in a subset of OC cells both in vitro and in vivo and supports angiogenesis.

Relaxin expression is induced by inflammatory cytokines in OC derived ascites.

HGSOCs originate in the secretory cells of the fallopian tube (31). Following oncogenic transformation, these cells disseminate into the peritoneal cavity, where they undergo metastatic colonization (2). The fallopian tube epithelium is an extraovarian source of relaxin, and expresses both *RLN1* and *RLN2* (32, 33). Expression of relaxin was observed in fallopian tube secretory cells (FT), OE6/E7 oviductal cells, and 9 of 12 ovarian cancer cell lines, but was undetectable in all 5 cell lines derived from normal ovarian epithelium (Figure 4A). Consistent with relaxin-*RXFP1* dependency in cancer cell survival and the non-tumorgenic potential of FT cells, shRNA knockdown of either *RXFP1* or *RLN* had no effects on cell viability in FT194 (Supplementary Figure S4A).

Relaxin expression was evaluated in primary HGSOC tumors and normal fallopian tube samples derived from the Canadian Ovarian Experimental Unified Resource (COUER) cohort. The analysis of relaxin expression included 73 primary HGSOC tumors and 9 normal fallopian tube samples. Analysis revealed relaxin expression in fallopian tube epithelium and HGSOC tumors, with a range of expression

observed in tumors (Figure 4B, Supplementary Figures S4B and S4C). Quantification revealed a larger but non-significant variation in relaxin expression in tumors compared to FT (Supplementary Figure S4D). Sera derived from a patient cohort consisting of HGSOC samples (n=38), clear cell carcinomas (n=3), other ovarian cancers (n=7) and control serum from healthy donors (n=14) were also evaluated (Supplementary Figure S4E). Relaxin levels were significantly higher in blood serum from the 48 OC patients relative to 14 normal controls (p=0.01) (Figure 4C).

Peritoneal ascites develops in two thirds of advanced stage ovarian cancers contributing extensively to morbidity (34). Malignant ascites is a reservoir of soluble factors which provide a pro-inflammatory and tumor-promoting microenvironment (35). Relaxin was detected in 10 of 11 patient-derived ascites supernatants by ELISA (Figure 4D). We conjectured that ascites may promote ovarian cancer progression, in part by inducing relaxin expression. Consistent with this, FT194 had increased levels of relaxin following growth in 10% ascites supernatant (Figure 4E) suggesting soluble factor(s) present in ascites may contribute to elevated relaxin.

IL-6 is among the most abundant cytokine in ascites and high levels predicts worse progression free survival in patients with advanced ovarian cancer (36–38). High IL-6 and TNF-α have been identified in a sub-group of patients which suggested an interaction between ascites IL-6 and TNF-α driving tumor progression and resistance to chemotherapy (36). High levels of IL-6 were confirmed in patient-derived ascites (Supplementary Figure S4F). Relaxin can stimulate macrophages to produce IL-6, suggesting that relaxin signaling in tumor cells could be initiated and sustained in the tumor microenvironment through interaction with immune cell effectors (39, 40). Relaxin stimulated OVCAR8 increased expression of *IL-6* mRNA in a dose dependent manner but no effect on *TNF* mRNA was observed (Figure 4F).

We hypothesized that relaxin/IL-6 constituted a feedback loop; therefore the effect of IL-6 on relaxin expression was examined. Relaxin levels increased in OVCAR8 following treatment with IL-6 and reached maximal expression in OVCAR8 and SKOV3 16-hours post treatment (Figures 4G and 4H). TNF-α treatment also increased relaxin expression in OVCAR8 (Figure 4G). Elevated *RLN1* mRNA was observed in OVCAR8 following IL-6 or TNF-α treatment, suggesting a transcriptional mechanism (Supplementary Figure S4G). Therefore, inflammatory cytokines may promote OC tumor progression through the induction of RLN expression.

The *RLN* promoter is regulated by cytokine induced activation of STAT3 and NFκB.

To understand the mechanism of RLN regulation by inflammatory cytokines, the promoters of *RLN1* and *RLN2* were examined. A series of genomic fragments surrounding the *RLN2* transcription start

site (TSS) were cloned into a pGL3 promoter-less luciferase plasmid (Figure 5A). *RLN2* was chosen over *RLN1* because it is more widely expressed. All constructs were functional in OVCAR8 and SKOV3, as demonstrated by high luciferase activity (Figure 5B). A minimal promoter (RP-3) containing several conserved DNA regions was the smallest fragment displaying robust activity. Consistent with a gene duplication event of relaxin genes, the *RLN2* RP-3 sequence is >90% conserved with the corresponding region in the *RLN1* promoter suggesting common transcriptional regulation of these two genes (Figure 5C).

To identify transcription factors (TF) regulating *RLN* expression, the RP-3 sequence was examined using *in-silico* TF binding prediction (ConSite and Match). Because RLN was induced by both IL-6 and TNF-α, we focused on TFs activated by these cytokines, STAT3 and NFκB, respectively. RP-3 contained several predicted STAT3 and NFκB elements, two of which mapped to peaks of high conservation (Figures 5A and 5C). A highly conserved binding site for SOX9, a protein of the high mobility group DNA-binding domain family was also present. Notably, the highly conserved STAT3 and SOX9 binding sites are present in the *RLN1* promoter (Figure 5C, Supplementary Figure S5A).

Knockdown of *STAT3* in multiple cells diminished luciferase expression from the RP-3 reporter (Figure 5D, Supplementary Figure S5B). Knockdown of *SOX9* decreased luciferase expression in SKOV3 and PEA2, but no change was observed in OVCAR8 (Figure 5D). Knockdown of *NFκB1* or *NFκB2* decreased luciferase activity in OVCAR8, SKOV3 and PEA2 (Figure 5E). In OVCAR8, *RLN1* mRNA was decreased with TF knockdown (Supplementary Figure S5C). STAT3 or the NFκB inhibition decreased relaxin expression in OVCAR8 concomitant with decreased phosphorylation of STAT3 and NFκB subunit RELA, respectively (Figure 5F).

Consistent with IL-6 induced STAT3 activation (41), the RP-3 luciferase activity was significantly increased by IL-6 treatment in both OVCAR8 and SKOV3 (Figure 5G). TNF-α stimulation activated the RP-3 reporter in OVCAR8 but not SKOV3. JAK1/2 or NFκB inhibition blocked the IL-6 and TNF-α induced relaxin in OVCAR8 confirming cytokine activation of TFs driving *RLN* expression (Figure 5H, Supplementary Figure S5D). Furthermore, application of ascites fluid to FT cell lines induced p-STAT3 levels consistent with ascites having high levels of IL-6 (Supplementary Figure S5E). To demonstrate that IL-6 is driving induction of relaxin, IL-6 neutralizing antibody was added to ascites and relaxin expression was suppressed (Supplementary Figure S5F). These results demonstrated that IL-6 in ascites induced RLN expression in OC cells through JAK/STAT pathway activation. Interestingly, 12/16 genes in the relaxin gene signature have a STAT3 binding element in their promoter, further supporting the relaxin autocrine signaling (Supplementary Figure S5H).

To validate occupancy of TFs on the endogenous *RLN* promoter, chromatin immunoprecipitation (ChIP) of STAT3, NFκB1, NFκB2, and SOX9 in OVCAR8, SKOV3 and PEA2 was performed. Distinct amplicons for ChIP were designed at the proximal promoters of both *RLN1* and *RLN2*. Binding of STAT3, NFκB1, NFκB2 and SOX9 were enriched on the *RLN1* promoter in all three cell lines (Figure 5I). IL-6 treatment increased binding of STAT3, while TNF-α treatment increased binding of STAT3, NFκB1 and SOX9 on the *RLN1* promoter in OVCAR8 (Supplementary Figure S5I). Interestingly, binding of STAT3, NFκB1, NFκB2, and SOX9 was detected on the *RLN2* promoter in PEA2 cells which express both *RLN1* and *RLN2* relative to OVCAR8 and SKOV3 which express predominantly *RLN1* (Figure 5J). In summary, STAT3, NFκB and SOX9 are transcriptional activators of *RLN* in multiple cell lines which are acting downstream of inflammatory cytokines (Supplementary Figure S5J).

The relaxin-RXFP1 autocrine loop contributes to cisplatin resistance via *RLN* promoter activation.

Activation of cytokine signaling can counteract chemotherapy and promote resistance (35). Since IL-6 and TNF-α are induced following cisplatin treatment and contribute to chemoresistance (42), we investigated whether relaxin-RXFP1 signaling contributes to cell survival following cisplatin treatment. *RXFP1*-dependent cell lines tended to be inherently more cisplatin resistant as determined by the cisplatin IC_{50} value (Figure 6A). The median cisplatin IC_{50} value was higher in *RXFP1*-dependent cell lines vs. independent cell lines (12.3 μM vs. 5.2μM, p=0.02). In addition, relaxin was significantly elevated in 9/12 patient serum samples following treatment with taxol/carboplatin (Supplementary Figure S6A and S6B) consistent with the idea that chemotherapy can induce relaxin expression in OC tumors as a survival adaption to the cytotoxic effects.

Increased IL-6 and TNF-α were measured in conditioned media from OVCAR8 and SKOV3 and activation of STAT3 and NFκB-P65 in OVCAR and SKOV3 cell lysates following treatment with cisplatin (Supplementary Figures S6C to S6E). Consistent with increased activation of relaxin regulating TFs following cisplatin treatment, RP-3 promoter activity and secretion of relaxin was increased in response to cisplatin exposure in both OVCAR8 and SKOV3 (Supplementary Figures S6F and S6G).

We reasoned that if induction of RLN is part of an adaptive response of OC cells to cisplatin, then depletion of RLN may increase cisplatin sensitivity. In SKOV3 and PEA2, knockdown of either *RXFP1* or RLN combined with sub-lethal doses of cisplatin significantly impacted cell growth compared to shGFP control (Figure 6B). Clonogenic colony assays revealed dramatically decreased colony formation upon treatment with a sub-lethal dose (2.5 μM) of cisplatin in combination with *RXFP1* or RLN knockdown (Figure 6C). Analysis of the coefficient of drug interaction (CDI)(43) revealed a synergist effect of *RXFP1*

or RLN knockdown combined with cisplatin treatment (SKOV3 CDI<0.27 and PEA2 CDI<0.33 for sh1-*RXFP1* or sh1-RLN and 2.5μM Cis; see methods).

We next tested if *RXFP1* knockdown sensitized tumor cells to cisplatin in vivo. Luciferase expressing OVCAR8 was derived that contained tetracycline-inducible sh1-*RXFP1* or shGFP and injected into the peritoneal cavity of NSG mice (Figure 6D). Two weeks following injection, mice were divided into sucrose alone or sucrose + Dox groups to induce shRNA expression. Three weeks post injection, mice were divided into cisplatin (1mg/kg once per week for 3 weeks) or vehicle treated groups (Figure 6D). The bioluminescence intensity in the TET-shGFP group with or without Dox increased rapidly and consistently from injection to week 5.5 (Figures 6E and 6F). Cisplatin treated TET-shGFP groups with or without Dox demonstrated slightly reduced tumor growth over the course of the experiment. Similar to the TET-shGFP control group, the non-induced TET-sh-*RXFP1* tumors grew with similar kinetics (Figures 6E and 6F). However, induction of TET-sh-*RXFP1* knockdown resulted in diminished tumor growth and near tumor eradication in the presence of cisplatin (Figures 6E to 6G). The combined effect of *RXFP1* knockdown and cisplatin treatment in vivo demonstrated a CDI=0.1 compared to a CDI=0.8 for the shGFP and cisplatin treatment control group. These results demonstrate potent sensitization of in vivo cisplatin-induced cytotoxicity by inhibition of RXFP1 expression.

Relaxin neutralizing antibody decreases OC viability and potentiates cisplatin cytotoxicity.

We hypothesized that relaxin neutralization would be deleterious to OC cell growth and potentiate cisplatin cytotoxicity. RLN1 and RLN2 peptides share 87% sequence identity within the primary receptor binding (B chain) domain and 63% identity within their secondary receptor binding (A chain) domain. A library of monoclonal antibodies (RLN2Am34) was generated aiming to identify clones that neutralize both RLN1 and RLN2 mediated cAMP induction. Supernatants derived from the RLN2Am34 library identified clones with strong binding to RLN2 and relatively weaker binding to RLN1 (Supplementary Figure 7A). Several clones bound both ligands and were tested for neutralization of relaxin in cell-based cAMP assays (Supplementary Figures S7B and S7C). Hybridoma clone m34-21 bound to both RLN1 and RLN2 and demonstrated potent RLN2 neutralization with favourable binding kinetics and a Kd in the low nM range (Supplementary Figure S7D). m34-21 reduced growth and viability of OVCAR8 in a dose-dependent manner but had no effect on OVCAR5 compared to monoclonal IgG1 kappa isotype control (Figures 7A to 7C).

To determine if neutralization of relaxin by m34-21 increases cisplatin sensitivity, OVCAR8 and OVCAR5 were treated with or without sub-lethal doses of cisplatin (1.75μM) in combination with m34-

21 (50µg/mL). Co-treatment blocked proliferation in cell culture over a 7 day period compared to OVCAR8 treated with only sub-lethal cisplatin or sub-lethal cisplatin plus isotype antibody control (Figure 7D). OVCAR5 showed no further growth impairment from m34-21 in combination with cisplatin.

To establish if any resistant cells were present after the 7 day treatment, cells were re-plated for colony formation assays following treatment with cisplatin or with the combined treatment of m34-21/cisplatin (Figure 7E). In OVCAR8, cisplatin or m34-21 treatment alone significantly reduced colony formation upon re-plating (Figure 7F). Strikingly, the combination of m34-21 and cisplatin completely abolished colony repopulation. A CDI=0.34 for OVCAR8 treated with both m34-21 and cisplatin versus a CDI=0.98 for the isotype control was calculated. OVCAR5 were not sensitive to any treatment (CDI>1.0 for all conditions). Therefore, neutralization of relaxin increased cisplatin sensitivity in *RXFP1*-dependent OC cells.

DISCUSSION

The emergence of autocrine loops is a strategy frequently exploited by tumors to proliferate autonomously, establish metastatic programs and adapt to the cytotoxic effects of chemotherapeutic drugs. Examples of autocrine signaling loops in ovarian cancer include PDGF-PDGFR, LPA-LPAR, FGF-FGFR, and FSH-FSHR ligand-receptor pairs (44–47). Here we report the identification of a relaxin-RXFP1 autocrine loop essential in sustaining survival and proliferation in a subset of ovarian cancer cells.

Relaxin protects against apoptosis through the activation of multiple signaling pathways including MAPK and AKT pathways. Transcriptome profiling revealed genes and pathways upregulated by relaxin that collectively sustain proliferation and cancer progression. Top enriched pathways included MAPK signaling, extracellular matrix receptor interaction, NOTCH, and VEGF signaling. Several RLN-upregulated genes encode for secreted factors, including macrophage migration inhibitory factor (*MIF*), MMPs (*MMP9*, *MMP23B* and *MMP15*), and *VEGF* that have potential to influence other cells in the tumor microenvironment. *NOTCH1* and *NOTCH3* were upregulated following relaxin treatment supporting emerging studies of the association between relaxin and Notch signaling. Considerable evidence supports an important oncogenic role of Notch signaling in HGSOC. Perturbation in the regulation of Notch-1 and Notch-3 as well as Notch ligands have been described, which has been linked to tumor initiation and progression, metastasis, stemness, and chemotherapy resistance (48, 49). The involvement of relaxin-RXFP1 in aberrant regulation of Notch signaling in ovarian cancer is therefore an important topic of future studies. Relaxin thus induces a transcriptional program that likely contributes to the survival, invasiveness and overall fitness of ovarian cancer.

Inflammatory cytokines such as IL-6 and TNF-α are central mediators of tumor progression in ovarian cancer. IL-6 has a central role in OC carcinogenesis and progression through its ability to stimulate invasion of cancer cells through increased expression of MMPs, stimulate the cell cycle, and promote epithelial to mesenchymal transition (50, 51). High level of IL-6 in the serum and ascites of cancer patients produced by monocytes/macrophages and malignant cells is associated with worse clinical outcome, peritoneal metastasis, and may play a key role in chemoresistance. Activation of STAT3 is reported to be an early event in the initiation of tumorigenesis within the fallopian tube epithelium and contributes to molecular changes that allow cells to survive in the presence of DNA damage (52). Our results show that *RLN* is a direct transcriptional target of IL-6 and TNF-α through the downstream TFs STAT3 and NFκB. The presence of relaxin in the fallopian tube epithelium and its regulation by IL-6/STAT3, coupled with its role in upregulating MMPs and survival pathways suggest that relaxin signaling could contribute to the downstream effects of IL-6/STAT3 in tumor promotion.

We identified a highly conserved SOX9 binding site in the proximal promoters of *RLN1* and *RLN2* and demonstrated SOX9 occupation on these promoters by ChIP. SOX9 promotes transcription of *RXFP2* in human embryonic fibroblast 293T cells and primary rat gubernacular cells (53). Thus, SOX9 may have a more widespread role in the regulation of relaxin-related peptides and receptors in reproductive development and disease. SOX9 is elevated in many types of cancer, including lung, skin, brain, and pancreatic cancers, and high expression correlates with disease progression, chemoresistance, and poor patient survival (54, 55). The complex role of RLN regulation by SOX9 will be an important topic for future study.

Cisplatin resistance is a net effect of multiple mechanisms that either trigger activation of pro-survival pathways or inhibition of cell death pathways (56). Several microenvironment-regulated signaling pathways mediate chemoresistance in ovarian cancer, including AKT, NFκB and STAT3 pathways (57). Elevated IL-6 levels in serum and ascites of EOC patients correlates with the emergence of chemoresistance, although the underlying mechanisms of IL-6-mediated chemoresistance in ovarian cancer cells are not completely understood. However, some studies showed that IL-6 is associated with increased expression of multidrug resistance-related genes, apoptosis inhibitory proteins (BCL2, BCLXL and XIAP) as well as activation of MAPK and PI3K/AKT signaling (58). Here, we identify relaxin-RXFP1 signaling as pro-survival mechanism induced by cisplatin treatment. We demonstrated that relaxin expression is increased following exposure to sublethal concentrations of cisplatin. In agreement with previous studies, cisplatin treatment also promoted increased secretion of both IL-6 and TNF-α.

Elevated expression of RLN protein was observed in several samples from ovarian cancer patient serum, tumors, and ascites. Our results corroborate a recent study that measured higher serum relaxin levels in patients with epithelial ovarian cancer versus those with benign ovarian diseases and healthy controls (59). Serum relaxin was associated with adverse prognosis, with increased levels correlating with FIGO stage, metastasis, survival, and chemoresistance. We detected increased relaxin levels in sera derived from HGSOC patients as well as patients with clear cell carcinomas and other ovarian cancers. This is consistent with our screening data across our panel of ovarian cancer cell lines. Although the large majority of lines in this panel were derived from HGSOC, several lines of different histological subtype also demonstrated dependency on RXFP1.

Our results demonstrate that targeting the relaxin-RXFP1 pathway may have therapeutic potential for treating a subset of OC patients, particularly in combination with standard platinum therapy and could potentially overcome chemoresistance of platinum resistant tumors.

METHODS

Source of primary samples: HGSOC tissue micro-array (TMA), formalin-fixed paraffin-embedded tissues was obtained from Centre hospitalier de l'Université de Montreal (CHUM). HGSOC tumors from 73 female patients were added to the TMA. Patients had no neo-adjuvant chemotherapy prior sample collection at surgery. Nine cases of normal fallopian tube tissues from women without gynaecological malignancy were added to the TMA as controls. Serum samples (Figure 4C) were obtained from the Penn Ovarian Cancer Research Center-BioTrust Collection. Serum samples (Supplementary Figure 6A and 6B) were obtained from CHUM.

Antibodies: AbCam Relaxin (ab183505). Cell Signaling Technologies AKT (9272), p-AKT (4056, 4058), BCL2 (a), Caspase3 (9662), cleaved-Caspase3 (9664), GAPDH (2118), MEK (4694), p-MEK (9154), PARP (9532), cleaved-PARP (9548), STAT (9139), p-STAT (9145) all at 1:1000 in 5% milk/PBST buffer. Santa Cruz β-actin (sc-8432), TUBULIN (sc-69969) at 1:3000.

Anti-relaxin mAB cell treatments: Cells were plated in 96 well plates at 3000 cells/well in RPMI (2% FBS). Immediately following plating, purified anti-relaxin monoclonal antibodies were added to each well at the indicated concentration. Cell growth was monitored using the INCUCYTE. For experiments testing combined treatment of anti-relaxin monoclonal antibodies and cisplatin (Sigma p4394), cells were plated as described above in the absence or presence of cisplatin (1.75μM) and mAB m34-21 (50μg/mL). Cells were re-plated from 96 wells to 12 wells for re-population assay following 7 day cisplatin exposure. Repopulating colonies were fixed in 4% paraformaldehyde and stained using 0.005% w/v crystal violet/

70% ethanol. Plates were scanned and quantified using ImageJ Colony Area Plug-in.

Anti-relaxin monoclonal antibodies: To generate monoclonal antibodies against Relaxin-2, four female BALB/c mice were immunized in a single hind footpad with synthetic RLN2 (Phoenix Peptide) in Ribi Adjuvant (Sigma Adjuvant System). Mice received booster injections (with adjuvant) twice weekly for 4 weeks. Serum was collected on day 21 to check titers by ELISA against Relaxin-2 and Relaxin-1 - all mice showed a strong serum response. Mice received a final boost of Relaxin-2 (PBS, no adjuvant) on day 28. Splenocytes and lymphocytes from mice were harvested on day 31. A hybridoma library (BALB/c "RLN2Am34") was created by PEG fusion of the pooled cells with P3X63Ag8.653 (CRL-1580) myeloma cells. After bulk HAT selection, the hybridoma library was cryopreserved.

Ascites Fluid Processing: Fluid was collected from HGSOC patients and processed within 24 hours. Fluid was centrifuged 300xg for 10 minutes at 4°C. To disrupt large clusters of cells/spheroids, pellets were suspended in PBS, filtered through sterile butter muslin and clusters greater than 70um were isolated. Isolated clusters were then dissociated with TrypLE Express (Invitrogen).

Bio-Layer Interferometry for kinetics: Binding kinetics between purified RLN2Am34-M21 ("m34-21") antibody and Relaxin-1 (RLN1) and Relaxin-2 (RLN2) were evaluated by bio-layer interferometry on the ForteBio Octet Red96. Purified m34-21 antibody was immobilized onto ForteBio Anti-Mouse-Fc Capture (AMC) biosensors (5μg/mL), followed by quenching of the AMC biosensors with irrelevant Mouse IgG (150μg/mL). After a baseline step, real time measurement of the association and dissociation of RLN1 and RLN2 was performed at 5 concentrations (111, 37.0, 12.3, 4.12 and 1.37nM). No significant binding of RLN1 to M21 was observed. On rates (k_{on}), off rates (k_{off}), and the overall molar affinity constant (K_D) for m34-21 binding to each concentration of RLN2 were calculated using a 1:1 model in Forte Bio Data Analysis software. A 1:1 Global K_D fit was also performed across multiple concentrations of each antigen, yielding a calculated K_D of M21 binding to RLN2 of 7.7E-10 (0.77nM).

BrdU assay: Cells were transfected with *RXFP1*-targeting siRNAs as described above. 24h post transfection, cells were plated in 96 well plates at a density of 5000 cells/well. Cells were serum starved for 16h and treated -/+ recombinant relaxin for 24h (n=3 per group). BrdU incorporation was measured according to the manufacturer's instructions (Cell Signaling Technology #6813) and absorbance was read at 450nM.

cAMP assay: Detection of cAMP, 5000 cells were seeded in 96 well plate in RPMI (10% FBS). 24 hours after seeding, cells were starved for 8 hours, pre-treated with 1mM IBMX (500uM, Stemcell Technologies 72762) for 2 hours and then treated +/- 50ng/mL recombinant human relaxin rhRLN2 (Phoenix Pharmaceuticals (035-62) for 30 minutes. Pelleted cells were suspended in 300μl 0.1M HCL for

10 minutes. cAMP levels were determined by ELISA according to the manufacturer's instructions (Enzo Life Sciences ADI-901-163).

Cell confluence and viability: 1-2x10^5 target cells were infected as indicated. Following selection with puromycin, cells were trypsinized, counted, and plated in 96-well plates at 2.0x10^3 cells/well. Cell confluence was monitored using an INCUCYTE™ Kinetic Imaging System (Essen BioScience) until shGFP expressing cells reached confluence. Viability was determined using PrestoBlue® (Thermo Fisher Scientific, A13261) according to the manufacturer's protocol.

Cell lines: OVCAR8, SKOV3, PEA1, PEA2, PEO4, PEO6 and OVCAR5 were obtained from the ATCC and cultured in RPMI 1640 with 10% fetal bovine serum. OAW42 was cultured in DMEM containing 20IU/L bovine insulin and 10% FBS. Information on all cell lines used for shRNA screening has been previously described (11). FT194 was maintained in DMEM/F12 containing 2% USG. Normal ovarian surface epithelial cell lines (NOV3198G, NOV3918G+C, NOV3202G, NOV3210, and NOV2309) were established as described previously (60)and maintained in OSE + 10% FBS. All cultures were maintained at 37°C in 5% CO2. Identity of all cell lines was validated by STR profiling, and each cell line was confirmed negative for mycoplasma.

Cell treatments: Cell lines were starved in RPMI containing 0% FBS for 16hr then treated with human recombinant RLN2 (50ng/mL, Phoenix Pharmaceuticals 035-62), hIL-6 (5-100ng/mL, CST 8904) or hTNFa (5-100ng/mL, CST 8902) for the indicated duration. For ascites coculture experiments, cells were starved and then cultured in serum free media containing 10% ascites for 72h in the absence or presence of αIL-6 neutralizing antibody (10μg/mL, R&D Systems AF-206-NA). For STAT3 and NFKB inhibition, cells were treated with Stattic (1μM, Selleckchem S7024) or QNZ (5nM, Selleckchem S4902) for 16-48hrs.

Cell-based relaxin ELISA: Following selection for shRNA constructs, 3000 cells were plated in complete media for 24hrs and then serum free media. After 72hrs, media was collected and protein levels measured by ELISA according to the manufacturer's instructions (Immunodiagnostik K9210).

Chromatin immunoprecipitation: ChIP was performed using SimpleChIP Enzymatic Chromatin IP kit with magnetic beads (Cell Signaling #9003) following the manufacturers' protocol. The following antibodies were used: anti-SOX9 (Santa Cruz Biotechnology, sc-166505X), anti-NFκB1 (Cell Signaling Technology, CST 13586S), anti-NFκKB2 (CST 37359), anti-STAT3 (Cell Signaling Technology, CST 9139S) and Control-IgG (Abcam, ab18413).

Clonogenic survival assay: Cells transduced with the indicated constructs plated at 2500 cells/well in 6 well plates. Saline or cisplatin (1, 2.5, and 5 μM, Sigma p4394) was added 48hr post plating. Following an additional 48hrs, 2500 cells from each treatment were re-plated in normal culture media (no cisplatin) and colonies were formed over 2-3 weeks. Cells were fixed and stained with 4% paraformaldehyde, 0.5% crystal violet in 20% methanol, washed and scanned.

Coefficient of drug interaction: CDI was performed as described (43). Briefly, the CDI is determined by the formula CDI=(A+B)/(AB), where A is the survival percentage of effect or treatment 1 and B is the survival percentage of effect or treatment 2. AB is the survival percentage of the combined effects or treatments. Percent survival is calculated using Alomar Blue assay, cell counting, or tumor flux as required per experiment using fixed ratio and different concentrations of cisplatin as indicated in each experiment.

Colony formation: $1.0x10^3$ cells were suspended in 0.5ml of 0.35% Bacto agar (BD, 214050) in growth media and plated on 0.5ml of 0.5% Bacto agar base in 12 well plates. The number of colonies (>50 cells) was scored after 2-3 weeks of incubation by first staining cells with 0.005%w/v crystal violet in 70% ethanol and counting the colonies by eye under a light microscope.

Flow cytometry: For apoptosis assays, cells were trypsinized, counted, washed in ice-cold PBS, and suspended in staining media (1xHBSS, 2%FBS, 2.5mM $CaCl_2$). Cells were transferred to polystyrene tubes, and $1.0x10^6$ cells were stained with 100μg/ml propidium iodide (PI, Santa Cruz Biotechnology 25535-16-4) and 5μl Annexin V-FITC (BD 556419) for 15 minutes at RT. Cells were suspended in 400μl staining media and fluorescence was measured using a Becton-Dickinson LSRII flow cytometer. FCS 3.0 files were analyzed using FlowJo version 9.2.

Hybridoma analysis by ELISA: Mouse sera, polyclonal supernatants from each hybridoma library, and monoclonal hybridoma supernatants after single cell cloning were analyzed using a coated antigen, anti-IgG reporter ELISA. EIA/RIA 96-well plates (Corning) were coated overnight (4°C) with either fixed concentrations or serial dilutions of Relaxin-1 (R&D Systems) or Relaxin-2 (Phoenix Peptide) diluted in 1X PBS. After blocking with PBS/Casein, plates were washed and incubated with serum (1/1000 dilution) or hybridoma supernatant (undiluted), followed by 1/5000 dilution of goat anti-Mouse IgG-HRP (Jackson ImmunoResearch), washed and incubated with TMB Substrate Solution (Moss Substrates) for 30 minutes. ELISA Stop Solution (1M H3PO4) was added to the wells and absorbance was measured at 450nm on an EnSpire microplate reader (PerkinElmer). Incubations were for 1.5-2hrs at ambient temperature. To isolate clones from the RLN2Am34 library, viable hybridoma cells were sorted via a BD

FACS Aria III, one cell per well, into 96-well plates (10-20 plates from each library). After 12 days in culture, monoclonal hybridoma conditioned supernatants from each 96-well plate were sampled for ELISA screening against RLN2. From ten 96-well plates from the RLN2Am34 library, 41 RLN2-binding clones were identified and 25 were selected for expansion and cryopreservation.

Hybridoma neutralizing activity analysis: THP-1 cells were suspended at $5x10^6$ cells/mL in RPMI (10%FBS) and pre-treated with IBMX for 30 minutes at 37°C. Pelleted cells were suspended in the absence or presence of 10ng/mL recombinant human RLN2 (Phoenix Pharmaceuticals (035-62) in hybridoma base media (DMEM) or hybridoma clonal supernatants (1mL total volume) and incubated for 20 minutes at 37°C. Pelleted cells were suspended in 300µl 0.1M HCL for 10 minutes. cAMP levels were determined by ELISA according to the manufacturer's instructions (Enzo Life Sciences ADI-901-163).

Immunoblotting: Cell lysates were prepared in RIPA buffer (50mM Tris-HCL [pH7.5], 150mM NaCl, 1% TritonX, 1% Na deoxycholate) containing 10mM NaF, 1mM Na_3VO_4 and 1mM PMSF with 1x Halt™ Protease Inhibitor cocktail (ThermoFisher). Lysates were incubated on a rotating plate at 4°C for 30 minutes, cleared by centrifugation and quantified using Pierce™ BCA Protein Assay Kit (Life Technologies). Cleared lysates were suspended in 2X sample buffer, boiled, and 20µg protein were resolved by SDS-PAGE and transferred to PVDF membranes. For experiments examining phosphorylated protein activation, cells were lysed directly in 2X sample buffer at the indicated time points. Membranes were blocked in 5% milk, washed 1xPBST and incubated with antibodies diluted in blocking buffer using standard protocols. Membranes were developed using ECL prime western blotting detection reagent (GE HealthCare Life Sciences) using the MicroChemi apparatus (DNR Bio-Imaging Systems). Densitometry of western blots was performed using Quantity One (BioRAD) software.

Immunofluoresence: TMA was deparaffinised at 60°C for 15-20 minutes and washed twice with toluene to remove residual paraffin. Antigen retrieval was performed using the BenchMark XT Ventana automated staining system (Ventana Medical Systems). Slides were incubated one hour at 37°C with primary antibodies directed against RLN2 (1:500, ab183505, Abcam), washed in PBS, blocked with blocking reagent (Dako), incubated with fluorescent secondary antibodies for 45 minutes at RT, washed in PBS, blocked overnight with Mouse On Mouse blocking reagent (MKB-2213, Vector laboratories) and incubated with antibodies directed against keratins (1:200, KRT7, MS-1352-P, Neomarkers; KRT18, sc-6259, Santa Cruz Biotechnology; KRT19, MS-198-P, Thermo Scientific) for 1hr at RT. Slides were quenched with 0.1%m/v Sudan Black in 70% ethanol for 15 minutes, washed, and mounted with Prolong Gold antifade containing DAPI (Molecular Probes, P36935). TMA slides were scanned with a 20X 0.75NA objective with a resolution of 0.3225um (VS110, Olympus, Center Valley, Pennsylvania). Fluorescent

intensities of RLN2 staining in the epithelial or stromal structures were quantified as mean fluorescence intensity (MFI) using Visiopharm® (VP) software (Visiopharm). For all markers, MFI dichotomization into high versus low expression was established using ROC curves (SPSS).

Lentivirus: $2.2x10^5$ HEK293T cells were co-transfected with 500ng packaging plasmid pPAX2, 50ng envelope plasmid VSV-G, and 500ng of shRNA-expressing pLKO.1 plasmid using XtremeGENE 9 (Roche), according to the manufacturer's protocol. 24hrs post transfection, media was replaced with DMEM (30% FBS) and cells were incubated for 24-48 hours. Lentiviral supernatants were collected, passed through a 0.45μm filter and stored at -80°C. Recipient cells were infected in media containing 6μg/mL polybrene (Sigma) for 24hrs, and incubated with growth media containing 5-10μg/mL puromycin (Bioshop) for 48h.

Organoids: HGSOC organoid models were generated by the Princess Margaret Living Biobank (PMLB) Organoid core facility. Dissociated cells were seeded at a density of 80,000 cells/well in 100% growth factor-reduced matrigel (VWR) on pre-warmed 24 well plates. Solidified domes were overlaid with ovarian growth media (DMEM/F12 supplemented with Glutamax, HEPES, Anti/Anti, 100ng/mL noggin, 1.25mM N-Acetylcysteine, 1 mM nicotinamide, 100ng/mL FGF10, 100ng/mL bFGF, 10 uM Rocki (Y27632), 20ng/mL EGF, 10mM Forskolin, 100nM 17-B-estradiol) and maintained in 37°C 5% CO_2. Cultures were passaged after 14-21 days, with media changes every 3-4 days. Matrigel and cells were dissociated with TrypLE Express for 20 min at 37°C and passaged at ratios of 1:1 to 1:4 into fresh matrigel. Organoid cultures and PDX models identities were matched to patient tissue by short tandem repeat (STR) analysis. Organoid cultures were routinely tested for *Mycoplasma* contamination. For IHC, **o**rganoid cultures were fixed in PFA and embedded in histogel (ThermoFisher Scientific). Tumour tissues embedded in paraffin, sliced into 4μm portions, dried overnight at 60°C and stained with antibodies using BenchMark XT autostainer (Ventana Medical Systems). Primary antibodies for IHC analysis were specific to AE1/AE3, p53 (DAKO), Pax8 (ProteinTech Group), and RXFP1 (Sigma HPA027067). Slides were imaged using an Aperio Scascope XT (Leica) microscope.

Pathway enrichment analysis: RLN2 upregulated gene set (log2FC>0.3, p<0.01) was processed using g:Profiler (g:Profiler version *e94_eg41_p11_88c9db6*, database updated on 24/01/2019). Output was subsequently visualized in Cytoscape (v3.7.1) using the Enrichment Map App. Depmap analysis of the dependency of ovarian cancer cell lines on the RLN2 regulated gene panel was conducted using the CRISPR (Avana) Public 19Q2 dataset. cBioportal for cancer genomics was used to query the alterations of the RLN2 regulated gene panel in clinical tumor samples and correlation with survival data obtained from TCGA.

PDX tissue processing: PDX model was generated from ascites collected as indicated above. 2 x10^7 cells were immersed in matrigel (10% matrigel in FBS-RPMI media) and implanted at the subcu site of NODSCID (Princess Margaret Living Biobank, UHN). PDX tumors were harvested at 1 cm diameter and processed immediately. The tissue was minced into 1 mm^2 pieces, washed with PBS and enzymatically dissociated with Liberase (Sigma) for half an hour at 37°C with agitation.

Plasmid cloning: Luciferase promoter vectors were cloned from digested PCR products amplified from human gDNA (Roche) into *KpnI/XhoI* cut pGL3-Basic Vector (Promega). Doxycycline-inducible sh*RXFP1* or control shRNA constructs were generated by annealing sense and antisense oligonucleotides followed by phosphorylation with T4 kinase and ligation into the AgeI/EcoRI sites of tet-on-pLKO vector.

Promoter luciferase assay: 7.0x10^4 cells/24 well were co-transfected with 50ng pRLN2-Luc or empty vector (pGL3-Basic, Promega) and 1ng phRL-SV40 (Promega) using Lipofectamine-2000 (Invitrogen) according to the manufacturer's instructions. 24h following transfection, cells were lysed and assayed for firefly and Renilla luciferase activity using the Dual-Luciferase Reporter System (Promega).

Quantitative PCR: RNA was extracted from cells using Trizol (ThermoFisher) according to the manufacturer's protocol. cDNA was synthesized from 0.5-1μg RNA using QuantiTect (QIAGEN). QPCR was performed using Fast SYBR® Green Master Mix (Life Technologies) or TaqMan™ Fast Advanced Master Mix.

RNA-seq analysis: OVCAR8 were starved in RPMI containing 0% FBS for 16hr then treated with human recombinant RLN2 (50ng/mL, Phoenix Pharmaceuticals 035-62) for 8hrs. RNA was extracted using Trizol. STAR (v2.4.2a) was used to quantify transcripts following RNA sequencing, using hg38 as the reference and Gencode (v25) for annotation. Differential analysis of quantified read counts from across the samples was facilitated by the DESeq2 package (v1.16.1) in the R statistical environment (v3.4.1). Transcripts with zero reads mapped across all samples were filtered out prior to downstream analysis. Read counts were then collapsed to gene level, which for the most part resulted in a one-to-one match. In the small fraction of cases where multiple transcripts existed, the transcript with the highest reads mapped was kept. To minimize noise and improve future validation success and efficiency, lowly-expressed genes were filtered out by applying a minimum sum of at least 10 reads mapped in total per gene across the six samples. Fold changes were generated from the filtered count data matrix, modelled as a function of condition (Vehicle vs. RLN2 treated) using the DESeq2 package, and p-values were further adjusted for multiple testing using a false discovery rate (FDR) of 1%. Significant hits were defined as genes with an FDR-adjusted p-value of at least 0.01 and an absolute log2-fold change greater than 1 between conditions.

siRNA: Cells were seeded at $1.0x10^5$ cells/well and transfected with 10nM siGenome SMARTpool targeting *RXFP1* (Thermo Fisher siGENOME SMARTpool® M-005649-01), or a non-targeting siRNA control (Thermo Fisher siGENOME SMARTpool®) or Silencer select siRNAs targeting *RXFP1* (Thermo Fisher # 4392420 assay ID s34026 and s34027) or control siRNAs (Thermo Fisher #4390843 or #4390846). Cells were transfected using DharmaFECT 1 reagent (Horizon Discovery T-2001-01), according to the manufacturer's protocol.

Tumor microvessel density: Paraffin-embedded tissues were sectioned (5µm), rehydrated, and antigen retrieval was performed using citrate buffer solution (Abcam:ab93684 Antigen Retrieval Buffer). Heat induced epitope retrieval was performed for 20 minutes at 98°C, cooled then washed in tap water for 5 minutes and blocked with serum free protein block (Dako Cat.No.X0909). Sections were incubated for 1hr at RT with primary antibody to detect CD31 (1:50, Rabbit anti-CD31, Abcam 28364), stained with biotinylated secondary (Anti-Rabbit Ig, Vector Labs BA-1000) for 30 minutes at RT. Detection was carried out with Avidin biotin complex system (Vector Labs PK-6100). Sections were incubated in DAB (Abcam:ab64238 DAB Substrate Kit) solution for 10 minutes. Samples were dehydrated, cleared in xylene and mounted. To assess MVD (microvessel density), CD31 positive clusters were counted at 20X magnification and were normalized to unit area.

Xenograft models: Xenografts were conducted in female NOD/SCID/IL2Rγ-/-(NSG) mice. $1.0x10^6$ cells in 100µl equal volume matrigel (BD, 354230) and 1xPBS were injected into the mammary fat pad (MFP) of three mice for a total of 6 per condition. Tumor measurements were taken biweekly and continued until tumor size reached 1.5 cm or became ulcerated. Tumors were removed, weighed, measured and fixed in 10% buffered formalin for histology or flash-frozen in liquid nitrogen. Tumor volume (V) was calculated by the formula $V = \pi/6 \times l \times w^2$, where l and w denote the longest and shortest diameter, respectively. For mice treated with doxycycline drinking water contained 1mg/mL doxycycline (Bio Basic). Animals in the untreated group were given water with 5% sucrose. For intraperitoneal xenograft assays, OVCAR8 were stably transduced with PKG-GFP-IRES-Luc vector and sorted for GFP-positive cells by flow cytometry. Cells were assessed for luciferase activity in vitro by treating with media containing 150µg/ml D-Luciferin (Perkin Elmer 122799) for 10 minutes and luminescence measured with GloMax®-Multi Detection System (Promega). Luciferase expressing cells were prepared for injection as described above. Tumor growth was monitored by injecting 10µl of D-Luciferin/gram body weight and bioluminescence imaged using the Xenogen IVIS Spectrum Imaging System (Perkin Elmer) in animals anesthetised with 2% isoflurane. Bioluminescence was quantified using the IVIS Live Image software (Caliper Life Sciences).

Statistics: A two-tailed Student's t test or Whitney-Mann U test was used to test significance in experimental conditions. Pairwise comparisons between treatment groups and a single control group were performed using Dunnett's test from the R package DescTools (v.0.99.38). P-values less than 0.05 were considered significant.

Data availability: The RNA-Seq dataset produced in this study is available in the following database: RNA-Seq data: Gene Expression Omnibus GSE151280 (https://www.ncbi.nlm.nih.gov/geo/query/acc.cgi?acc=GSE151280).

Study approval

All experiments using human samples and animal studies were carried out following ethical approval. In the case of human samples, written informed consent was obtained from participants prior to inclusion in this study. Written consent was obtained from all patients prior to sample collection. Participants are not identified by name. For human samples, ethical approval was obtained from the (CHUM) institutional ethics committee (Comité d'éthique de la recherche du CHUM). Experimental mice received environmental enrichment. Animal rooms are maintained at 20-24^{o}C, 40-65% humidity, and 12hr light/dark cycle. All animal studies were approved by the Animal Research Council of the University Health Network (Toronto, Ontario, Canada).

AUTHOR CONTRIBUTIONS

Conceptualization HB, RR; Methodology HB, LC, OAK, RS, KB, KF; Data Management HB, LC, OAK, RS, KB; Writing – Original Draft HB, OAK, RR; Writing – Review and Editing HB, OAK, KF, RR; Funding Acquisition HB, RR; Resources AMMM, RD, RR; Supervision RR.

ACKNOWLEDGEMENTS

This research was supported by a CIHR Foundation grant, BioCanRX Catalyst grant, Cancer Research Society operating grant, and a grant from the Princess Margaret Foundation. This study used resources provided by the Canadian Ovarian Cancer Research Consortium's biobank funded by the Terry Fox Research Institute (grant no. 2012-46). AMMM is a researcher at CHUM, which receives support from the FRQS. We thank UHN animal and STARR facilities for assistance with Xenogen and Napoleon Law at STARR for help with IHC.

REFERENCES

1. Dong A, Lu Y, Lu B. Genomic/epigenomic alterations in ovarian carcinoma: Translational insight into clinical practice. *J. Cancer* 2016;7(11):1441–1451.

2. Lengyel E. Ovarian cancer development and metastasis. *Am. J. Pathol.* 2010;177(3):1053–1064.

3. Bast RC, Hennessy B, Mills GB. The biology of ovarian cancer: new opportunities for translation. [Internet]. *Nat. Rev. Cancer* 2009;9(6):415–28.

4. Yap TA, Carden CP, Kaye SB. Beyond chemotherapy: Targeted therapies in ovarian cancer. *Nat. Rev. Cancer* 2009;9(3):167–181.

5. O'Hayre M et al. The emerging mutational landscape of G proteins and G-protein-coupled receptors in cancer. *Nat. Rev. Cancer* 2013;13(6):412–424.

6. Liu Y et al. G protein-coupled receptors as promising cancer targets. *Cancer Lett.* 2016;376(2):226–239.

7. Bathgate R a D et al. Relaxin family peptides and their receptors. [Internet]. *Physiol. Rev.* 2013;93:405–80.

8. Marshall SA, Senadheera SN, Parry LJ, Girling JE. The Role of Relaxin in Normal and Abnormal Uterine Function during the Menstrual Cycle and Early Pregnancy. *Reprod. Sci.* 2017;24(3):342–354.

9. Dessauer CW, Nguyen BT. Relaxin stimulates multiple signaling pathways: Activation of cAMP, PI3K, and PKCζ in THP-1 cells. *Ann. N. Y. Acad. Sci.* 2005;1041:272–279.

10. Thanasupawat T et al. Emerging roles for the relaxin/RXFP1 system in cancer therapy. *Mol. Cell. Endocrinol.* 2019;487:85–93.

11. Medrano M et al. Interrogation of Functional Cell-Surface Markers Identifies CD151 Dependency in High-Grade Serous Ovarian Cancer. *Cell Rep.* 2017;18(10):2343–2358.

12. Marcotte R et al. Essential gene profiles in breast, pancreatic, and ovarian cancer cells. *Cancer Discov.* 2012;2(2):172–189.

13. Domcke S, Sinha R, Levine DA, Sander C, Schultz N. Evaluating cell lines as tumour models by comparison of genomic profiles. *Nat. Commun.* 2013;4:2126.

14. Beaufort CM et al. Ovarian cancer cell line panel (OCCP): Clinical importance of in vitro

morphological subtypes. *PLoS One* 2014;9(9):e103988.

15. Halls ML, Van Der Westhuizen ET, Bathgate RAD, Summers RJ. Relaxin family peptide receptors - Former orphans reunite with their parent ligands to activate multiple signalling pathways. *Br. J. Pharmacol.* 2007;150(6):677–691.

16. Rodgers LH, hAinmhire E, Young AN, Burdette JE. Loss of PAX8 in high-grade serous ovarian cancer reduces cell survival despite unique modes of action in the fallopian tube and ovarian surface epithelium. *Oncotarget* 2016;7(22):32785–32795.

17. Pontén F, Jirström K, Uhlen M. The Human Protein Atlas - A tool for pathology. *J. Pathol.* 2008;216(4):387–393.

18. Unemori EN et al. Relaxin induces vascular endothelial growth factor expression and angiogenesis selectively at wound sites. *Wound Repair Regen.* 2000;8(5):361–370.

19. Ahmad N, Wang W, Nair R, Kapila S. Relaxin induces matrix-metalloproteinases-9 and -13 via RXFP1: Induction of MMP-9 involves the PI3K, ERK, Akt and PKC-ζ pathways. *Mol. Cell. Endocrinol.* 2012;363(1–2):46–61.

20. Meyers RM et al. Computational correction of copy number effect improves specificity of CRISPR-Cas9 essentiality screens in cancer cells. *Nat. Genet.* 2017;49(12):1779–1784.

21. Dempster JM et al. Extracting Biological Insights from the Project Achilles Genome-Scale CRISPR Screens in Cancer Cell Lines. *bioRxiv* [published online ahead of print: 2019]; doi:10.1101/720243

22. Ghandi M et al. Next-generation characterization of the Cancer Cell Line Encyclopedia. *Nature* 2019;569(7757):503–508.

23. Cerami E et al. The cBio Cancer Genomics Portal: An open platform for exploring multidimensional cancer genomics data. *Cancer Discov.* 2012;2(5):401–404.

24. Gao J et al. Integrative analysis of complex cancer genomics and clinical profiles using the cBioPortal. *Sci. Signal.* 2013;6(269). doi:10.1126/scisignal.2004088

25. Bell D et al. Integrated genomic analyses of ovarian carcinoma. *Nature* 2011;474(7353):609–615.

26. Halls ML, Bathgate RAD, Sutton SW, Dschietzig TB, Summers RJ. International union of basic and clinical pharmacology. XCV. Recent advances in the understanding of the pharmacology and biological roles of relaxin family peptide receptors 1–4, the receptors for relaxin family peptides. *Pharmacol. Rev.*

2015;67(2):389–440.

27. Bruell S et al. Chimeric RXFP1 and RXFP2 receptors highlight the similar mechanism of activation utilizing their N-terminal low-density lipoprotein class A modules. *Front. Endocrinol. (Lausanne).* 2013;4(NOV). doi:10.3389/fendo.2013.00171

28. Sudo S et al. H3 relaxin is a specific ligand for LGR7 and activates the receptor by interacting with both the ectodomain and the exoloop 2. *J. Biol. Chem.* 2003;278(10):7855–7862.

29. Radestock Y, Willing C, Kehlen A, Hoang-Vu C, Hombach-Klonisch S. Relaxin enhances S100A4 and promotes growth of human thyroid carcinoma cell xenografts. *Mol. Cancer Res.* 2010;8(4):494–506.

30. Neschadim A et al. Relaxin receptor antagonist AT-001 synergizes with docetaxel in androgen-independent prostate xenografts. *Endocr. Relat. Cancer* 2014;21(3):459–471.

31. Lee Y et al. A candidate precursor to serous carcinoma that originates in the distal fallopian tube. *J. Pathol.* 2007;211(1):26–35.

32. Tang XM, Chegini N. Human fallopian tube as an extraovarian source of relaxin: Messenger ribonucleic acid expression and cellular localization of immunoreactive protein and 125I-relaxin binding sites. *Biol. Reprod.* 1995;52(6):1343–1349.

33. Rouillard AD et al. The harmonizome: a collection of processed datasets gathered to serve and mine knowledge about genes and proteins. *Database (Oxford).* 2016;2016. doi:10.1093/database/baw100

34. Ahmed N, Stenvers KL. Getting to know ovarian cancer ascites: Opportunities for targeted therapy-based translational research. *Front. Oncol.* 2013;3 SEP. doi:10.3389/fonc.2013.00256

35. Kim S, Kim B, Song YS. Ascites modulates cancer cell behavior, contributing to tumor heterogeneity in ovarian cancer. *Cancer Sci.* 2016;107(9):1173–1178.

36. Kolomeyevskaya N et al. Cytokine profiling of ascites at primary surgery identifies an interaction of tumor necrosis factor-α and interleukin-6 in predicting reduced progression-free survival in epithelial ovarian cancer. *Gynecol. Oncol.* 2015;138(2):352–357.

37. Macciò A, Madeddu C. Inflammation and ovarian cancer. *Cytokine* 2012;58(2):133–147.

38. Browning L, Patel MR, Horvath EB, Tawara K, Jorcyk CL. IL-6 and ovarian cancer: Inflammatory cytokines in promotion of metastasis. *Cancer Manag. Res.* 2018;10:6685–6693.

39. Horton JS, Yamamoto SY, Bryant-Greenwood GD. Relaxin modulates proinflammatory cytokine

secretion from human decidual macrophages. *Biol. Reprod.* 2011;85(4):788–797.

40. Horton JS, Yamamoto SY, Bryant-Greenwood GD. Relaxin augments the inflammatory IL6 response in the choriodecidua. *Placenta* 2012;33(5):399–407.

41. Tempfer C et al. Serum evaluation of interleukin 6 in ovarian cancer patients. *Gynecol. Oncol.* 1997;66(1):27–30.

42. Jones VS et al. Cytokines in cancer drug resistance: Cues to new therapeutic strategies. *Biochim. Biophys. Acta - Rev. Cancer* 2016;1865(2):255–265.

43. Zhao Y et al. Cytotoxicity enhancement in MDA-MB-231 cells by the combination treatment of tetrahydropalmatine and berberine derived from Corydalis yanhusuo W. T. Wang. *J. Intercult. Ethnopharmacol.* 2014;3(2):68.

44. Matei D et al. Autocrine activation of PDGFRα promotes the progression of ovarian cancer. *Oncogene* 2006;25(14):2060–2069.

45. Xu Y. Lysophospholipid signaling in the epithelial ovarian cancer tumor microenvironment. *Cancers (Basel).* 2018;10(7). doi:10.3390/cancers10070227

46. Clayton NS, Wilson AS, Laurent EP, Grose RP, Carter EP. Fibroblast growth factor–mediated crosstalk in cancer etiology and treatment. *Dev. Dyn.* 2017;246(7):493–501.

47. Gera S et al. Follicle-stimulating hormone is an autocrine regulator of the ovarian cancer metastatic niche through notch signaling. *J. Endocr. Soc.* 2019;3(2):340–357.

48. Groeneweg JW, Foster R, Growdon WB, Verheijen RHM, Rueda BR. Notch signaling in serous ovarian cancer. *J. Ovarian Res.* 2014;7(1). doi:10.1186/s13048-014-0095-1

49. Brzozowa-Zasada M et al. Notch and its oncogenic activity in human malignancies. *Eur. Surg. - Acta Chir. Austriaca* 2017;49(5):199–209.

50. Wang Y et al. Interleukin-6 signaling regulates anchorage-independent growth, proliferation, adhesion and invasion in human ovarian cancer cells. *Cytokine* 2012;59(2):228–236.

51. Coward J et al. Interleukin-6 as a therapeutic target in human ovarian cancer. In: *Clinical Cancer Research*. 2011:6083–6096

52. Saini U et al. STAT3/PIAS3 levels serve as “early signature” genes in the development of high-grade serous carcinoma from the fallopian tube. *Cancer Res.* 2018;78(7):1739–1750.

53. Feng S et al. Developmental expression and gene regulation of insulin-like 3 receptor RXFP2 in mouse male reproductive organs. *Biol. Reprod.* 2007;77(4):671–680.

54. Jo A et al. The versatile functions of Sox9 in development, stem cells, and human diseases. *Genes Dis.* 2014;1(2):149–161.

55. Matheu A et al. Oncogenicity of the developmental transcription factor Sox9. *Cancer Res.* 2012;72(5):1301–1315.

56. Siddik ZH. Cisplatin: Mode of cytotoxic action and molecular basis of resistance. *Oncogene* 2003;22(47 REV. ISS. 6):7265–7279.

57. Pogge von Strandmann E, Reinartz S, Wager U, Müller R. Tumor–Host Cell Interactions in Ovarian Cancer: Pathways to Therapy Failure. *Trends in Cancer* 2017;3(2):137–148.

58. Wang Y et al. [Chemotherapy resistance induced by interleukin-6 in ovarian cancer cells and its signal transduction pathways].. *Zhonghua Fu Chan Ke Za Zhi* 2010;45(9):691–698.

59. Guo X et al. Serum relaxin as a diagnostic and prognostic marker in patients with epithelial ovarian cancer. *Cancer Biomarkers* 2017;21(1):81–87.

60. Lounis H et al. Primary cultures of normal and tumoral human ovarian epithelium: A powerful tool for basic molecular studies. *Exp. Cell Res.* 1994;215(2):303–309.

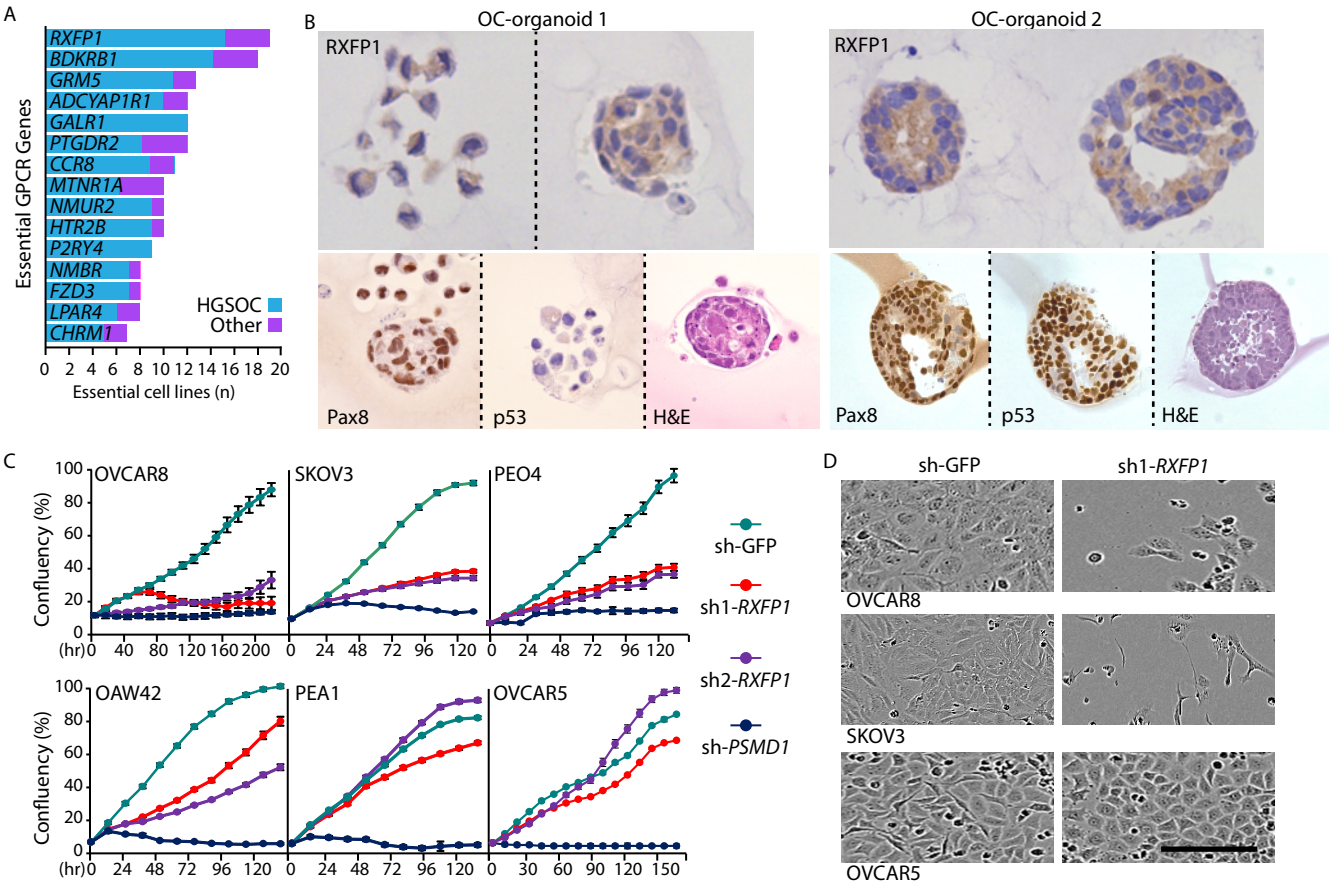
A
Essential GPCR Genes
RXFP1
BDKRB1
GRM5
ADCYAP1R1
GALR1
PTGDR2
CCR8
MTNR1A
NMUR2
HTR2B
P2RY4
NMBR
FZD3
LPAR4
CHRM1
HGSOC
Other
0 2 4 6 8 10 12 14 16 18 20
Essential cell lines (n)
B
OC-organoid 1
OC-organoid 2
RXFP1
Pax8
p53
H&E
C
OVCAR8
SKOV3
PEO4
OAW42
PEA1
OVCAR5
Confluency (%)
(hr)
sh-GFP
sh1-RXFP1
sh2-RXFP1
sh-PSMD1
D
sh-GFP
sh1-RXFP1
OVCAR8
SKOV3
OVCAR5
E
OVCAR8
SKOV3
GFP sh1 sh2 GFP sh1 sh2
MW (kDa)
cl-PARP
1.0 1.9 4.1 1.0 1.3 2.0
PARP
cl-CASP3
1.0 2.1 3.2 1.0 6.4 2.5
CASP3
BCL2
1.0 0.4 0.2 1.0 0.5 0.6
GAPDH
75
135
20
17
35
25
35
F
sh-GFP
sh1-RXFP1
sh2-RXFP1
OVCAR8 10 2 3
SKOV3 12 6 5
OVCAR5 6 5 6
G
UT
+Dox
Viability (%)
n.s
***
***
TET-sh-GFP
TET-sh1-RXFP1
TET-sh-PMSD1
H
UT
Dox D0
Dox D21
TET-sh-GFP
TET-sh1-RXFP1
I
TET-sh-GFP
TET-sh1-RXFP1
UT
Dox D0
Dox D21
Tumor Volume (mm3)
n.s.
***
*
Dox
Week
J
TET-sh-GFP
TET-sh1-RXFP1
Tumor Volume (mm3)
n.s
***
*
UT
D0
D21

Figure 1.

Figure 1. *RXFP1* is an essential GPCR in OC cell lines.

(A) GPCRs identified by shRNA screening. Genes are arranged by number of dependent cell lines based on significance of the normalized zGARP score (<0.05). Other represents clear cell or unknown origin.

(B) RXFP1, Pax8 and TP53 staining in OC organoids. (20X magnification, n=2).

(C) Growth of cell lines constitutively expressing shRNA control (shGFP), shRNAs targeting *RXFP1* (sh1-*RXFP1* or sh2-*RXFP1*) or targeting *PSMD1* (sh-*PSMD1*). Data points represent mean ± SEM. (n=3).

(D) Images of OVCAR8, SKOV3 and OVCAR5 72 hours post infection with the indicated constitutively expressed shRNAs. Scale bar 5μm. (

(E) Analysis of apoptosis in OVCAR8 and SKOV3 constitutively expressing shGFP (GFP) or shRNA targeting *RXFP1* (sh1 or sh2) 72 hours post infection.

(F) Soft agar growth of cells constitutively expressing shGFP or shRNA targeting *RXFP1* (sh1 or sh2). Average colony counts are indicated; also see Supplementary Figure 1G. Scale bar 100μm. (n=3).

(G) Viability of OVCAR8 expressing Doxycycline-inducible TET-shGFP, TET-sh1-*RXFP1* or TET-sh-*PSMD1* in the absence or presence of Doxycycline (+Dox, 1μg/mL) compared to untreated cells (UT). Results represent mean ± SEM (n=3). (Student's t-test, ***p<0.001; n.s.=not significant).

(H) OVCAR8 derived xenografts expressing Doxycycline-inducible control TET-shGFP or TET-sh1-*RXFP1*. Doxycycline was initiated on day of cell injection (D0) or 21 days post injection (D21).

(I) Analysis of OVCAR8 xenograft tumor measurement. Arrow indicates when Doxycycline (Dox) treatment was initiated (21 days post-injection). Results represent mean ± SEM (n=4). (Student's t-test, *p<0.05, ***p<0.00001, n.s.=not significant)

(J) Final mean volume (± SEM) of tumors described in (I). (Student's t-test ,*p<0.05, ***p<0.001).

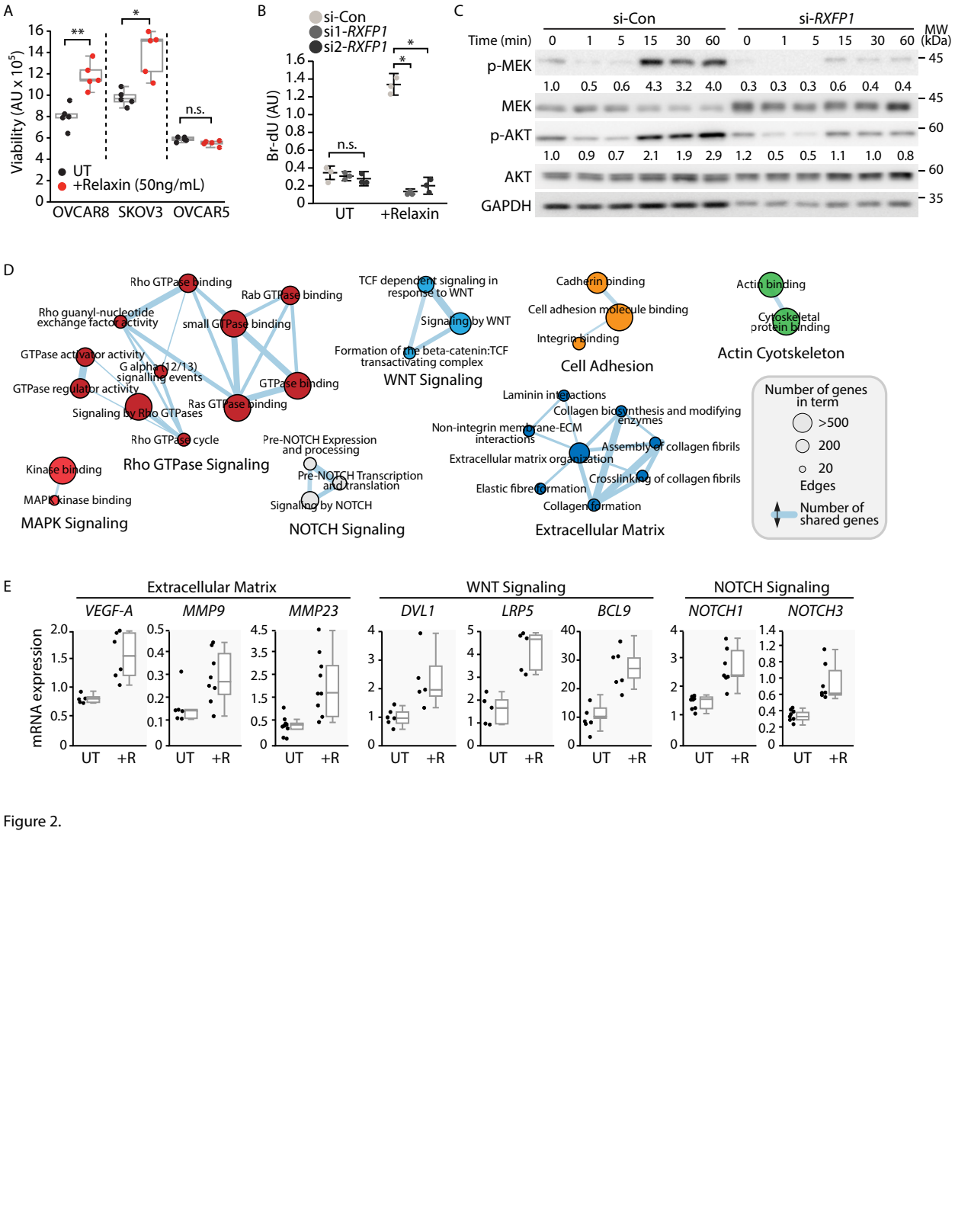
A
Viability (AU x 10^5)
UT
+Relaxin (50ng/mL)
OVCAR8
SKOV3
OVCAR5
n.s.
B
si-Con
si1-RXFP1
si2-RXFP1
Br-dU (AU)
n.s.
UT
+Relaxin
C
si-Con
si-RXFP1
Time (min)
MW (kDa)
p-MEK
MEK
p-AKT
AKT
GAPDH
D
Rho GTPase binding
Rab GTPase binding
Rho guanyl-nucleotide exchange factor activity
small GTPase binding
GTPase activator activity
G alpha (12/13) signalling events
GTPase regulator activity
GTPase binding
Signaling by Rho GTPases
Ras GTPase binding
Rho GTPase cycle
Rho GTPase Signaling
Kinase binding
MAPK kinase binding
MAPK Signaling
TCF dependent signaling in response to WNT
Signaling by WNT
Formation of the beta-catenin:TCF transactivating complex
WNT Signaling
Pre-NOTCH Expression and processing
Pre-NOTCH Transcription and translation
Signaling by NOTCH
NOTCH Signaling
Cadherin binding
Cell adhesion molecule binding
Integrin binding
Cell Adhesion
Laminin interactions
Collagen biosynthesis and modifying enzymes
Non-integrin membrane-ECM interactions
Assembly of collagen fibrils
Extracellular matrix organization
Crosslinking of collagen fibrils
Elastic fibre formation
Collagen formation
Extracellular Matrix
Actin binding
Cytoskeletal protein binding
Actin Cyotskeleton
Number of genes in term
>500
200
20
Edges
Number of shared genes
E
Extracellular Matrix
WNT Signaling
NOTCH Signaling
VEGF-A
MMP9
MMP23
DVL1
LRP5
BCL9
NOTCH1
NOTCH3
mRNA expression
UT
+R

Figure 2.

Figure 2. Relaxin initiates signaling pathways and gene activation.

(A) Cell viability in the absence (UT, untreated) or presence of recombinant human RLN2 (+ Relaxin, 50 ng/mL) for 24h. Results represent absorbance unit (AU) measurements (n=5, mean ± SEM). (Student's t-test, *p<0.05, **p<0.01, n.s.=not significant).

(B) BrdU incorporation in OVCAR8 in the absence (UT, untreated) or presence of recombinant RLN2 (+Relaxin, 50ng/mL) following transfection with control siRNA (siCON) or 2 different siRNAs targeting *RXFP1* (si1-*RXFP1 and* si2-*RXFP1*). Results represent absorbance unit (AU) measurements (n=3, mean ± SEM).

(C) Analysis of phosphorylated MEK (p-MEK) and AKT (p-AKT) in OVCAR8 treated with human RLN2 (50ng/mL) following transfection with siRNA control (siCON) or si-*RXFP1*.

(D) Significantly enriched pathways identified by RNA-seq (FDR Q value <0.01) in RLN2 treated OVCAR8. Nodes represent enriched pathways and edges the number of genes overlapping between two pathways. Enrichment analysis was carried out using g-profiler and visualized using Cytoscape.

(E) QPCR analysis of the indicated mRNA transcripts in untreated cells (UT) or cells treated with RLN2 (+R, 50ng/mL for 8 hours). Data points represent individual wells/replicates. Box plots indicate the IQR of the data and the central line shows the median. (n ≥ 5).

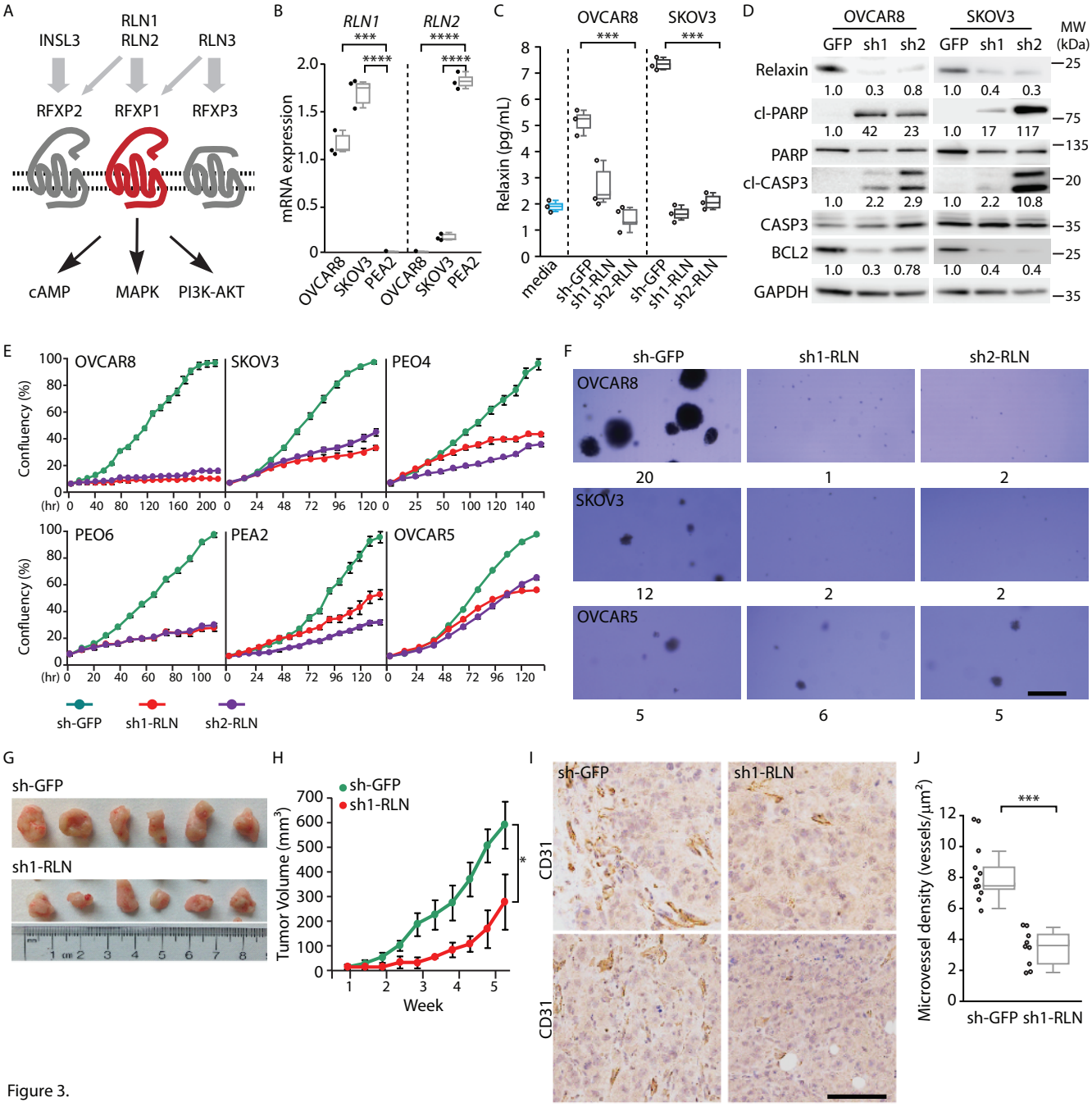
A
INSL3
RLN1
RLN2
RLN3
RFXP2
RFXP1
RFXP3
cAMP
MAPK
PI3K-AKT
B
RLN1
RLN2
mRNA expression
OVCAR8
SKOV3
PEA2
C
OVCAR8
SKOV3
Relaxin (pg/mL)
media
sh-GFP
sh1-RLN
sh2-RLN
D
OVCAR8
SKOV3
GFP
sh1
sh2
MW (kDa)
Relaxin
cl-PARP
PARP
cl-CASP3
CASP3
BCL2
GAPDH
E
OVCAR8
SKOV3
PEO4
PEO6
PEA2
OVCAR5
Confluency (%)
(hr)
sh-GFP
sh1-RLN
sh2-RLN
F
sh-GFP
sh1-RLN
sh2-RLN
OVCAR8
SKOV3
OVCAR5
G
sh-GFP
sh1-RLN
H
sh-GFP
sh1-RLN
Tumor Volume (mm3)
Week
I
sh-GFP
sh1-RLN
CD31
J
Microvessel density (vessels/μm2)
sh-GFP
sh1-RLN

Figure 3.

Figure 3. Expression of relaxin in OC cell lines is essential for survival.

(A) Schematic of relaxin signaling via RXFP receptors (1, 2, 3) and ligands (RLN1/RLN2/RLN3/INSL3) summarizing ligand specificity, relative potency and reported cross reactivity.

(B) mRNA levels of relaxin-1 (*RLN1*) and relaxin-2 (*RLN2*) in OVCAR8, SKOV3 and PEA2. For panels B and C, box plots indicate the IQR of the data and the central line shows the median. (Student's t-test ,***p<0.001, ****p<0.0001).

(C) Relaxin levels in media derived from OVCAR8 and SKOV3 constitutively expressing shGFP or shRNA targeting RLN (sh1- or sh2-RLN) 120h following selection. (n=3). (Student's t-test ,***p<0.001).

(D) Analysis of pro-relaxin and apoptosis related factors in OVCAR8 and SKOV3 constitutively expressing shGFP or shRNA targeting RLN (sh1- or sh2-) 48 hours following selection. Cleaved PARP (cl-PARP) cleaved Caspase-3 (cl-CASP3).

(E) Growth of OC cell lines constitutively expressing shGFP or shRNA targeting RLN (sh1- or sh2-RLN). Data represents mean ± SEM (n=3).

(F) Soft agar growth of cell lines expressing shGFP or shRNA targeting RLN (sh1- or sh2-RLN). Average colony counts are indicated; also see Supplementary Figure 3G. Scale bar 100µm. (n=3).

(G) Tumors derived from OVCAR8 expressing shGFP or sh1-RLN.

(H) Growth curves of tumors described in (G). (Student's t-test ,*p<0.02).

(I) Representative images of CD31 IHC in shGFP control and sh1-RLN expressing tumors. Scale bar 10µm.

(J) Quantification of microvessel density (CD31 positive clusters per unit area) in CD31 enriched regions within tumors expressing shGFP (n=11 regions) or sh1-RLN (n=9 regions). Box plots indicate the IQR of the data and the central line shows the median. (Student's t-test,***p<0.0001).

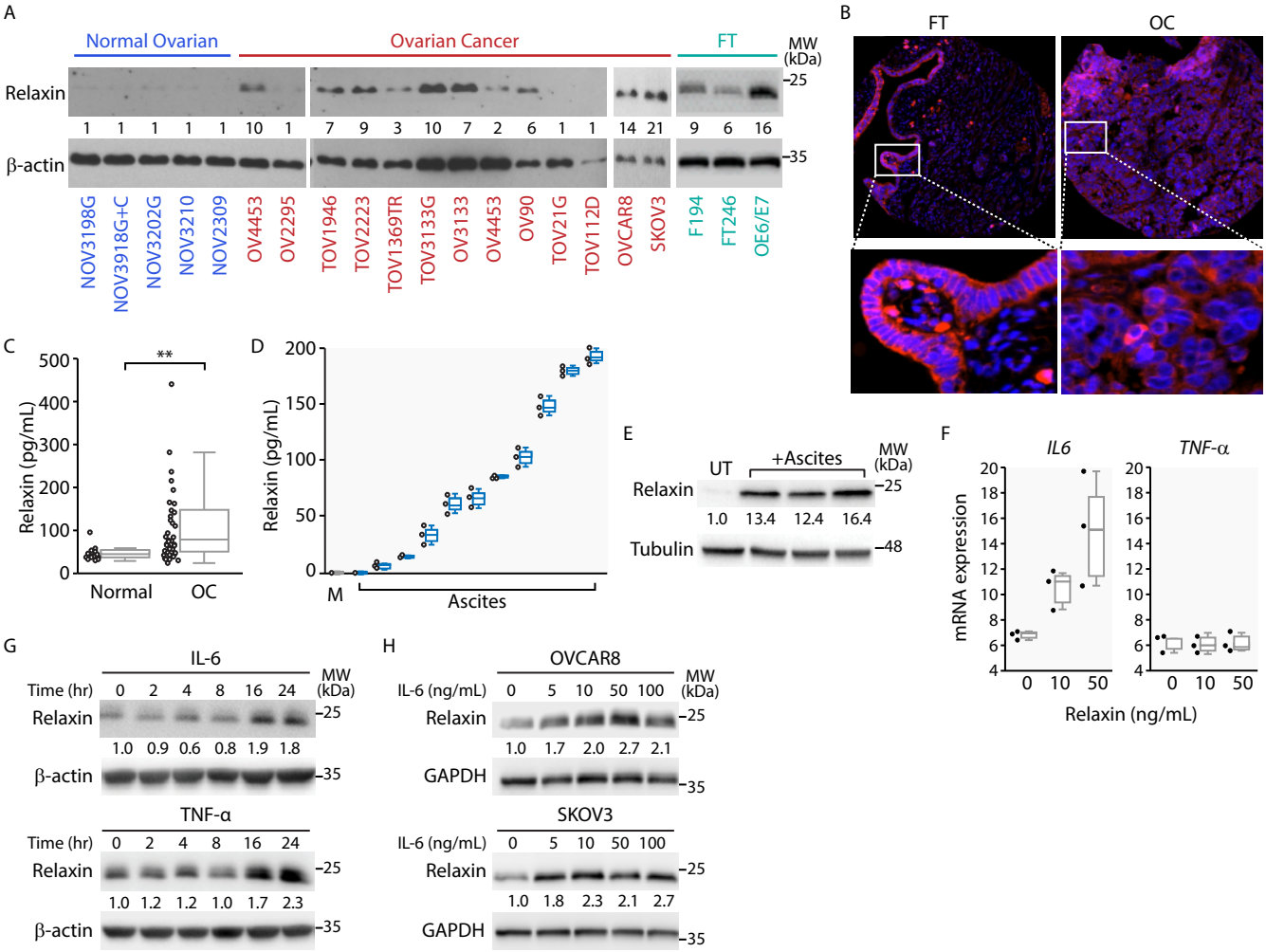
A
Normal Ovarian
Ovarian Cancer
FT
MW (kDa)
Relaxin
β-actin
NOV3198G
NOV3918G+C
NOV3202G
NOV3210
NOV2309
OV4453
OV2295
TOV1946
TOV2223
TOV1369TR
TOV3133G
OV3133
OV4453
OV90
TOV21G
TOV112D
OVCAR8
SKOV3
F194
FT246
OE6/E7
B
FT
OC
C
Relaxin (pg/mL)
Normal
OC
D
Relaxin (pg/mL)
M
Ascites
E
UT
+Ascites
Relaxin
Tubulin
F
IL6
TNF-α
mRNA expression
Relaxin (ng/mL)
G
IL-6
Time (hr)
TNF-α
β-actin
H
OVCAR8
IL-6 (ng/mL)
SKOV3
GAPDH

Figure 4.

Figure 4. Analysis of relaxin expression in patient-derived OC tumors, serum and ascites.

(A) Relaxin expression in normal ovarian, fallopian tube (FT) and OC cell lines. OV4453 is duplicated as it served as a positive control. Densitometry analysis rounded to the nearest whole number.

(B) Relaxin expression (red) in normal fallopian tube (FT) and HGSOC tissue samples.

(C) Relaxin levels (pg/mL) in sera derived from patients with epithelial OC (n=48) and healthy donors (normal, n=14). For this and subsequent panels, box plots indicate the IQR of the data and the central line shows the median. (**p=0.01 Student's t-test).

(D) Relaxin (pg/mL) in patient-derived ascites compared to tissue culture media (M). (n=3).

(E) Analysis of relaxin expression in FT194 cultured for 72h in media containing 10% ascites (+Ascites).

(F) IL-6 and TNF-α mRNA levels following treatment of OVCAR8 with RLN2 (50 ng/mL) for 24h. (n=3).

(G) Analysis of relaxin expression in OVCAR8 treated with IL-6 (50ng/mL) or TNF-α (50ng/mL).

(H) Analysis of relaxin expression in OVCAR8 and SKOV3 treated for 24h with increasing doses of IL-6 (ng/mL).

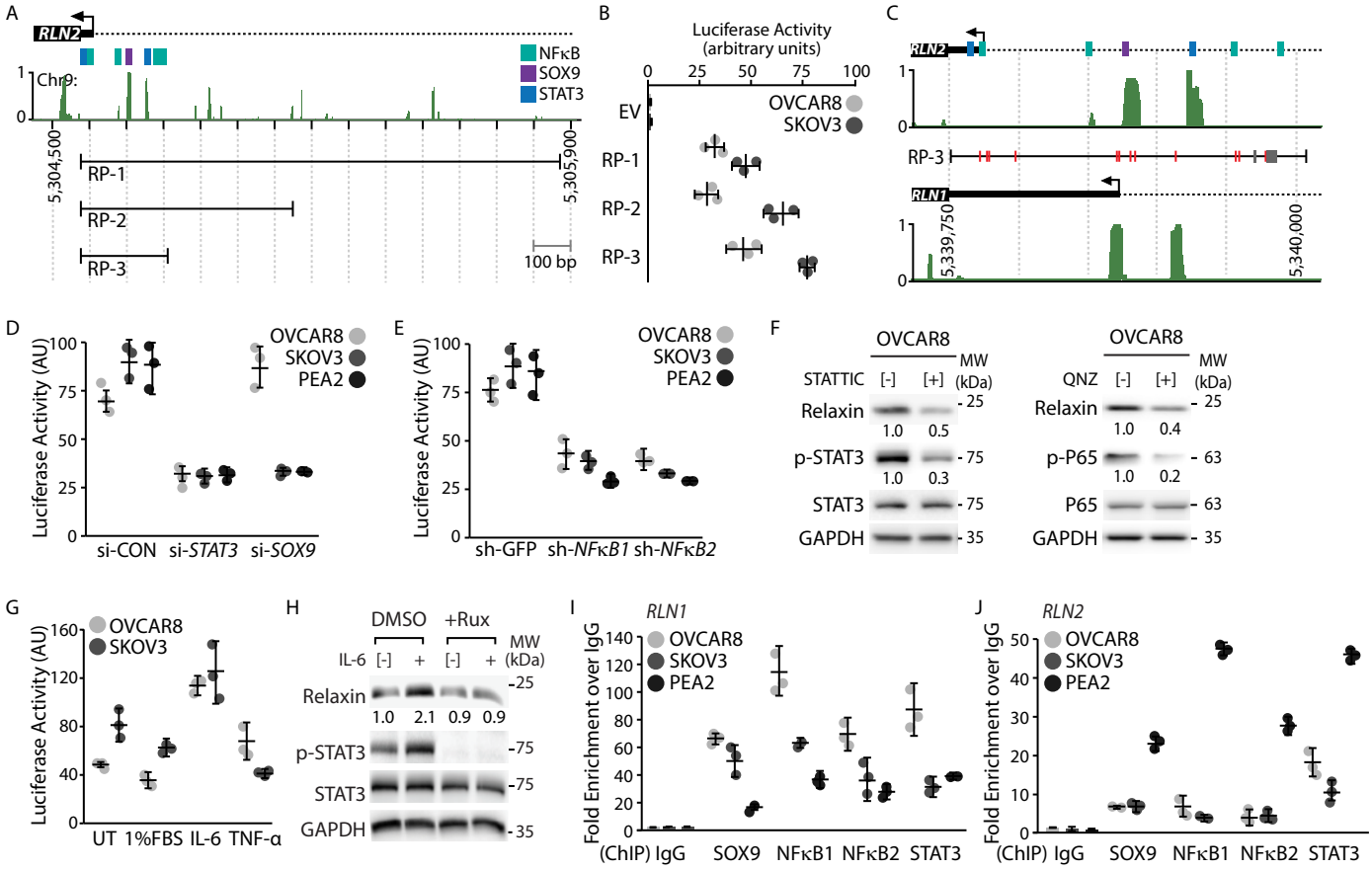
A
RLN2
NFκB
SOX9
STAT3
Chr9:
5,304,500
5,305,900
RP-1
RP-2
RP-3
100 bp
B
Luciferase Activity (arbitrary units)
EV
RP-1
RP-2
RP-3
OVCAR8
SKOV3
C
RLN2
RP-3
RLN1
5,339,750
5,340,000
D
Luciferase Activity (AU)
OVCAR8
SKOV3
PEA2
si-CON
si-STAT3
si-SOX9
E
sh-GFP
sh-NFκB1
sh-NFκB2
F
OVCAR8
STATTIC
QNZ
MW (kDa)
Relaxin
p-STAT3
STAT3
GAPDH
p-P65
P65
G
UT
1%FBS
IL-6
TNF-α
H
DMSO
+Rux
IL-6
I
RLN1
Fold Enrichment over IgG
(ChIP) IgG
SOX9
NFκB1
NFκB2
STAT3
J
RLN2

Figure 5.

Figure 5. The relaxin promoter is activated by STAT3 and NFκB.

(A) Schematic of the genomic region proximal to the *RLN2* transcriptional start site (UCSC genome browser-human GRCh37/hg19). Species conservation is indicated. Boundaries of three relaxin promoter (RP) constructs RP-1, RP-2 and RP-3 are mapped. Predicted binding sites for STAT3, NFκB and SOX9 are indicated.

(B) Luciferase activity of the indicated RP constructs compared to empty vector control (EV) in OVCAR8 and SKOV3. Luciferase activity is normalized to Renila activity. For this and subsequent experiments, error bars indicate mean ± SEM (n=3).

(C) Genomic region of the *RLN2* promoter (RP-3) compared to the *RLN1* promoter. Peaks indicate species conservation. Red bars in the RP-3 sequence indicate single nucleotide differences in *RLN1* compared to *RLN2* and the open box indicates a small sequence not present in *RLN1*. Predicted binding sites for STAT3, NFκB and SOX9 are indicated.

(D) RP-3 luciferase activity in cells transfected with control siRNA (siCON) or siRNA targeting *STAT3* or *SOX9*. (n=3).

(E) RP-3 luciferase activity in cells expressing shGFP or hairpins targeting *NFκB1* or *NFκB2* subunits (sh-NFκB1 and sh-NFκB2). (n=3).

(F) Relaxin expression and STAT3 phosphorylation (pY705) in OVCAR8 treated for 48h with small molecule inhibitors of STAT3 (STATTIC, 1μM) or NFκB (QNZ, 5nM) compared to mock treated (-) cells.

(G) RP3-luciferase activity in OVCAR8 and SKOV3 treated with 1%FBS, IL-6 (50ng/mL) or TNF-α (50ng/mL) for 24h compared to untreated (UT) cells. (n=3).

(H) Relaxin levels and STAT3 phosphorylation (pY705) in OVCAR8 treated with IL-6 (50ng/mL) or control (-) 24h post-treatment with the JAK1/2 inhibitor Ruxolitinib (+Rux) compared to DMSO.

(I, J) ChIP analysis of transcription factor occupancy at the *RLN1* promoter (I) and *RLN2* promoter (J). ChIP signals are fold enrichment over IgG (n=3).

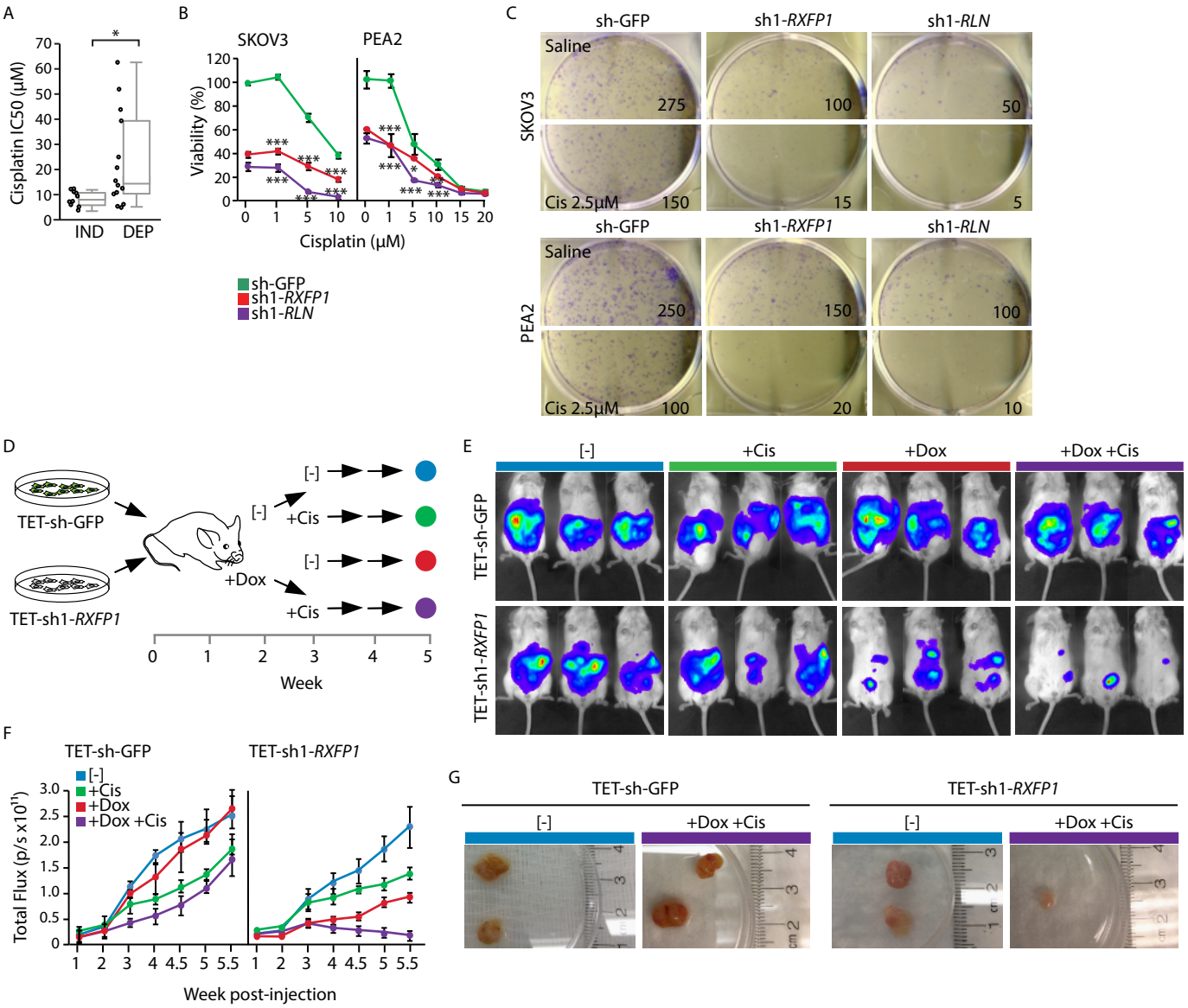
A
Cisplatin IC50 (µM)
IND
DEP
B
SKOV3
PEA2
Viability (%)
Cisplatin (µM)
sh-GFP
sh1-RXFP1
sh1-RLN
C
sh-GFP
sh1-RXFP1
sh1-RLN
Saline
Cis 2.5µM
SKOV3
PEA2
275
100
50
150
15
5
250
150
100
100
20
10
D
TET-sh-GFP
TET-sh1-RXFP1
[-]
+Cis
+Dox
Week
E
[-]
+Cis
+Dox
+Dox +Cis
TET-sh-GFP
TET-sh1-RXFP1
F
TET-sh-GFP
TET-sh1-RXFP1
[-]
+Cis
+Dox
+Dox +Cis
Total Flux (p/s x10^11)
Week post-injection
G
TET-sh-GFP
TET-sh1-RXFP1
[-]
+Dox +Cis

Figure 6.

Figure 6. *RXFP1* and relaxin knockdown sensitizes HGSOC cells and tumors to cisplatin.

(A) Cisplatin IC50 values (μM) in *RXFP1* independent (IND, n=10) and *RXFP1* dependent (DEP, n=14) cell lines. Box plots indicate the IQR of the data and the central line shows the median. (*p<0.00578 Wilcox Rank test, critical U=48 at p<0.5).

(B) Viability of SKOV3 and PEA2 expressing shGFP control or shRNA targeting *RXFP1* (sh1-*RXFP1*) or relaxin (sh1-RLN) and treated with increasing doses of cisplatin (μM). (Dunnett's test ,*p<0.03, **p<0.002, ***p<0.001, red and purple lines are compared to the green line).

(C) Clonogenic assay of cells expressing shGFP control or sh1-*RXFP1* sh1-RLN in the absence (saline) or presence of a sub-lethal dose of cisplatin (2.5μM). Quantification of colonies per images indicated.

(D) Scheme for testing combined effects of Doxycycline-induced *RXFP1* knockdown and cisplatin treatment in vivo. Luciferase expressing OVCAR8 co-expressing TET-inducible shRNA control (TET-shGFP) or TET-inducible shRNA targeting *RXFP1* (TET-sh1-*RXFP1*) were injected into the interperitoneal cavity of NSG mice. At week two mice were treated with sucrose control (-) or Doxycycline (+Dox) to initiate shRNA expression. At week 3, mice were divided into untreated (-) or cisplatin treated (+Cis, 1mg/kg per week) which was continued for three weeks. Color dots at the end point of the experiment mark the conditions: blue (-), green (-Dox, +Cis), red (+Dox, -Cis) and purple (+Dox, +Cis).

(E) Bioluminescence images of mice bearing intraperitoneal xenografts of OVCAR8 expressing TET-shGFP or TET-sh1-*RXFP1* in treatment groups 5-weeks post injection.

(F) Quantification of bioluminescence from xenografts expressing TET-shGFP or TET-sh1-*RXFP1*. Luminescence measurements expressed as total flux (photons/s). Error bars indicate mean ± SEM. (n=3).

(G) Representative tumors of OVCAR8 expressing TET-shGFP or TET-sh1-*RXFP1* extracted at the experimental endpoint showing the blue (-) and purple (+Dox, +Cis) groups.

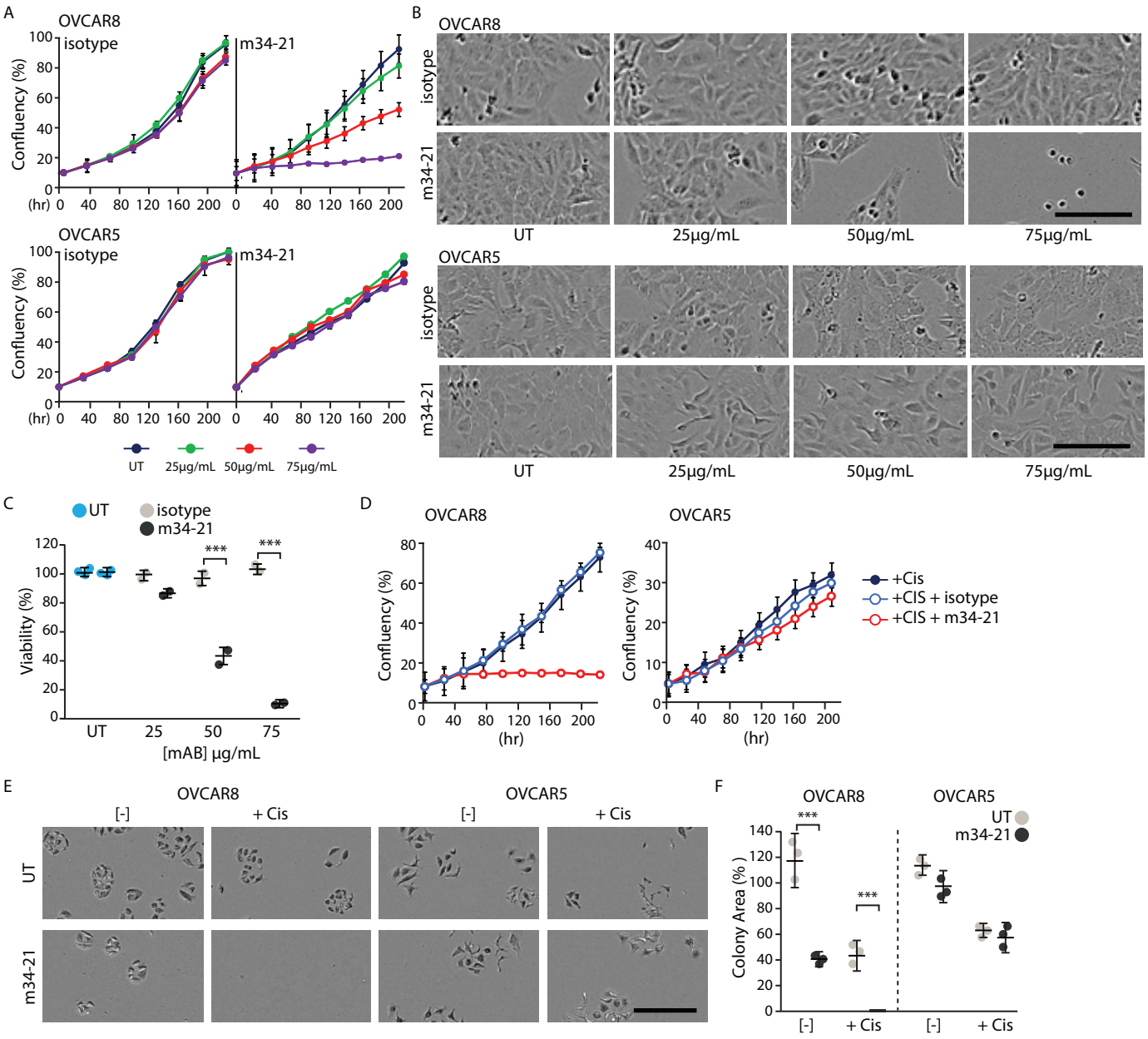
A
OVCAR8
isotype
m34-21
Confluency (%)
(hr)
OVCAR5
UT
25µg/mL
50µg/mL
75µg/mL
B
OVCAR8
isotype
m34-21
UT
25µg/mL
50µg/mL
75µg/mL
OVCAR5
C
UT
isotype
m34-21
Viability (%)
***
[mAB] µg/mL
D
OVCAR8
OVCAR5
Confluency (%)
(hr)
+Cis
+CIS + isotype
+CIS + m34-21
E
OVCAR8
OVCAR5
[-]
+ Cis
UT
m34-21
F
OVCAR8
OVCAR5
UT
m34-21
Colony Area (%)
***
[-]
+ Cis

Figure 7.

Figure 7. Relaxin neutralizing monoclonal antibody abrogates HGSOC cell growth.

(A) Growth of OVCAR8 and OVCAR5 treated with relaxin neutralizing monoclonal antibody (m34-21) or isotype control. Error bars indicate mean +/- SEM (n=5).

(B) Representative images of OVCAR8 and OVCAR5 treated with m34-21 or isotype control for 7 days. Scale bar 10μm. (n=5).

(C) Viability of OVCAR8 treated with m34-21 or isotype control for 7 days. For panels C and F, box plots indicate the IQR of the data and the central line shows the median. (n=5). (Student's t-test ,***$p<0.001$).

(D) Growth of OVCAR8 and OVCAR5 treated with a sublethal dose of cisplatin (1.75μM) alone or in combination with m34-21 or isotype control (50μg/mL). (n=5).

(E) Repopulating colonies formed following no treatment (-) or treatment with cisplatin (+Cis) alone (UT) or in combination with m34-21 (50μg/mL). Scale bar 10μm. (n=5).

(F) Quantification of the repopulating colony assay as described in (E). Quantification was performed using ImageJ. (Student's t-test ,***$p<0.001$, n=5).

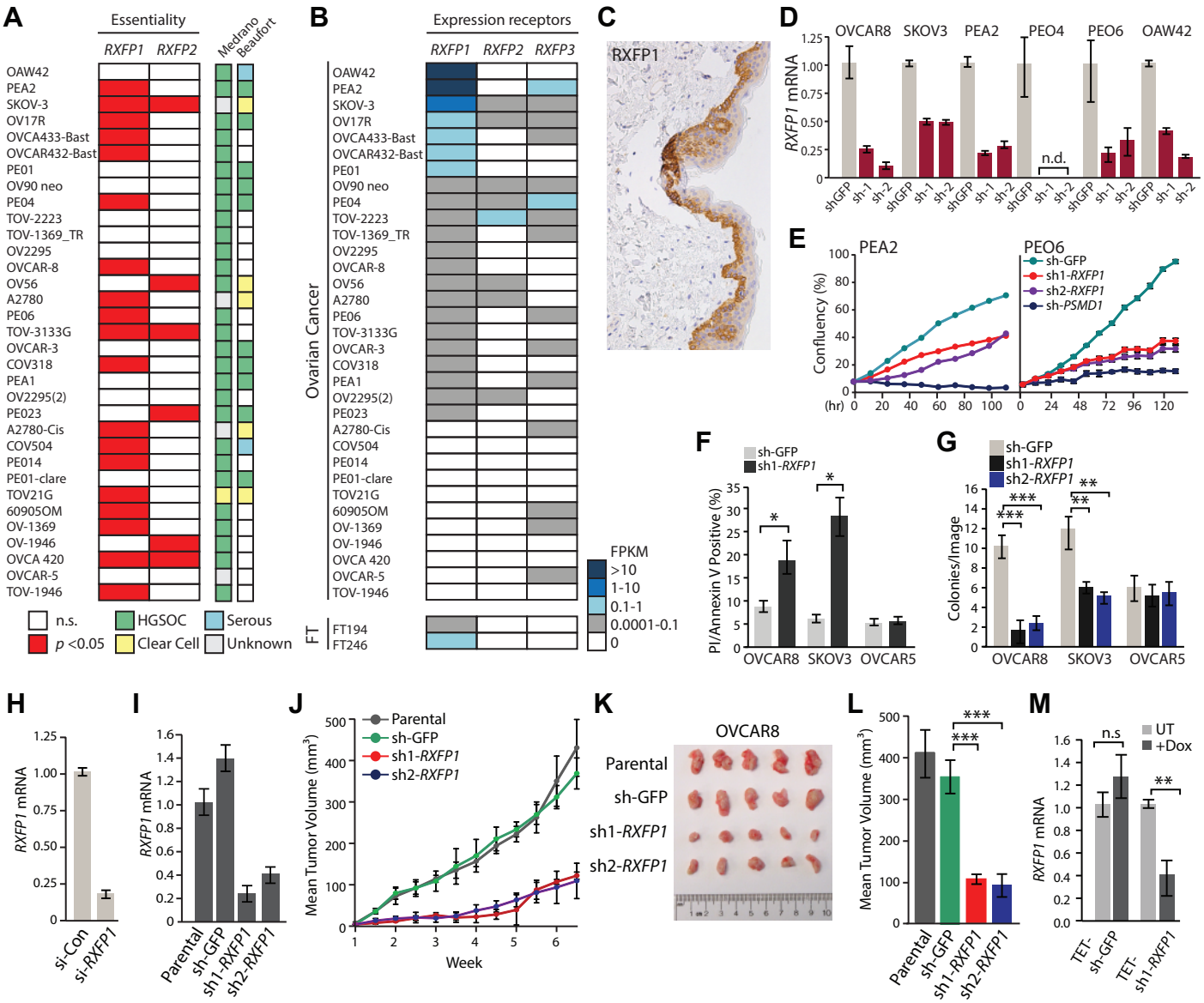

Fig.S1. *RXFP1* is an essential GPCR in a subset of HGSOC cell lines. Related to Fig.1.

(A) Essentiality score (p-value of GARP) for cell line dependency on *RXFP1* or *RXFP2*. P-value <0.05 considered essential (n.s. = not significant). Cell lines ranked based on expression of *RXFP1* (panel B). Origin of cell lines based on the suitability score (Medrano et al. Cell Reports, 2017) and putative histolgy (Beaufort et al. Plosone 2014).

(B) Representation of RNAseq expression values (FPKM) for relaxin receptors in ovarian cancer and fallopian tube (FT) cell lines.

(C) Postive control for RXFP1 staining by IHC . Human mucosa scamous epithelial cells stained with anti-RXFP1 antibody (Sigma Prestige).

(D) Validation of shRNA knockdown of *RXFP1* using two independent shRNAs targeting *RXFP1*(sh1-or sh2) or control (sh-GFP) in the indicated cell lines. For this panel and subsequent panels all shRNA are constitutively expressed.

(E) Growth curves of PEA2 and PEO6 expresssing control hairpins (sh-GFP or sh-*PSMD1*) or hairpins targeting *RXFP1* (sh1-*RXFP1* or sh2-*RXFP1*) as indicated in the legend.

(F) PI/Annexin V staining by flow cytometry 48 hours after puromycin selection in the indicated cell lines expressing sh-GFP or sh1-*RXFP1*. Error bars indicate mean ± SEM(n=3). (*p<0.01, student's t-test).

(G) Quantification of colonies formed in Fig.1E. Error bars indicate mean ± SEM (n=3). (*p<0.001, ***p<10E-06, Dunnett's test).

(H) *RXFP1* mRNA expression in OVCAR8 cells transfected with non-targeting control siRNA (si-Con) or siRNA targeting *RXFP1*.

(I) Validation of *RXFP1* knockdown in xenograft-injected OVCAR8 cells expressing constitutively active sh-GFP or two independent hairpins targeting *RXFP1* (sh1-*RXFP1*, sh2-*RXFP1*) in comparison to the parental cell line.

(J) Growth curves of the indicated OVCAR8 xenografts in mammary fat pad (error bars indicate mean +/- SEM; n=4).

(K) Excised xenografts from parental OVCAR8 or OVCAR8 expressing sh-GFP or shRNA targeting *RXFP1* (sh1-*RXFP1*, sh2-*RXFP1*).

(L) Mean tumor volume of excised xenografts described in (K). (***p<0.0001, Dunnett's test).

(M) Normalized expression (± SEM) of *RXFP1* mRNA in OVCAR8 cells expressing doxycycline-inducibleTET-shGFP or TET-sh1-*RXFP1* in the absence or presence of doxycycline (+Dox, 1 μg/mL) compared to untreated cells (UT) 48 hours post Dox treatment. (**p<0.001, student's t-test).

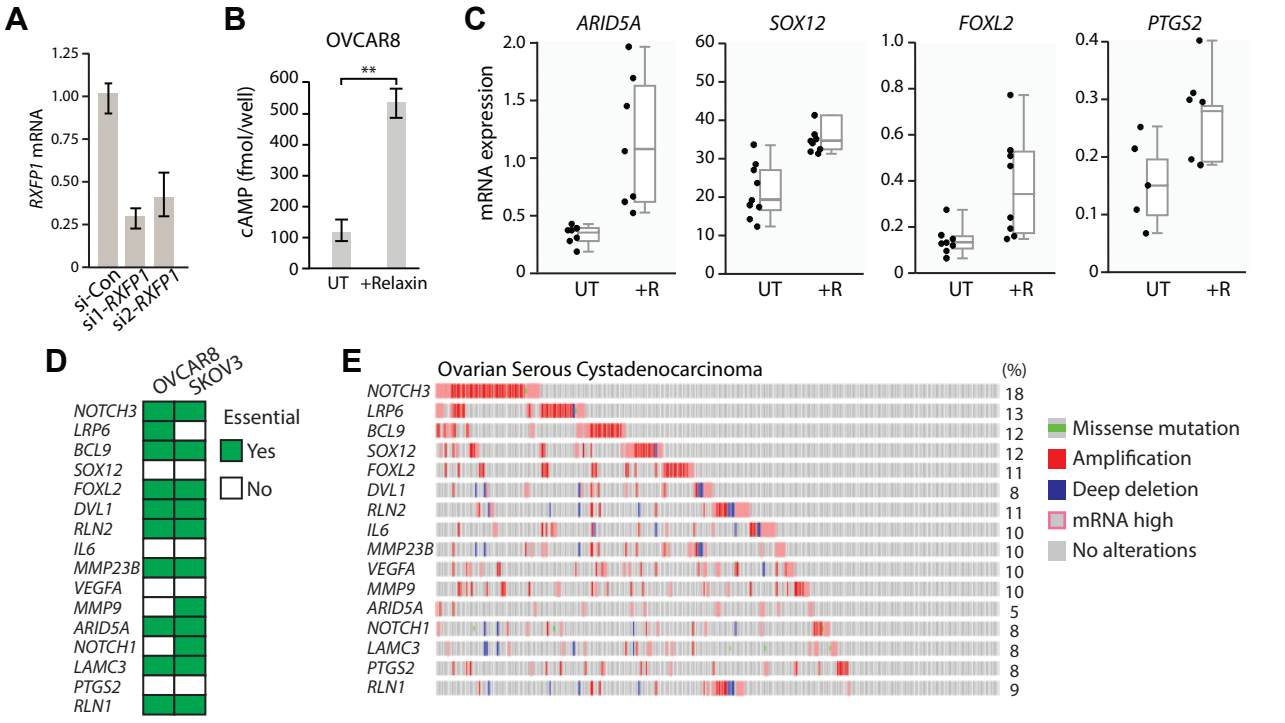

Fig.S2. Relaxin promotes proliferation and signaling in HGSOC cell lines. Related to Fig.2.

(A) *RXFP1* mRNA expression in OVCAR8 cells transfected with non-targeting control siRNA (si-Con) or siRNA targeting *RXFP1*.

(B) cAMP induction by recombinant human relaxin (+Relaxin) compare to untreated (UT) OVCAR8 cells. OVCAR8 cells were cultured in media containing low serum (1% FBS) overnight and were pre-treated with1mM IBMX for 2 hours at 37°C. Cells were cultured +/- human relaxin (50 ng/mL) for 30 minutes at 37°C. Cells were lysed and cAMP was measured by ELISA. Error bars indicate mean ± SD (n=3). (**p<0.001, student's t-test).

(C) Validation of selected relaxin target genes identified by RNAseq analysis. Transcript levels of each gene were measured in untreated cells (UT) or cells treated with recombinant human relaxin (+R, 50ng/mL) for 8h. Error bars indicate mean ± SD (n≥5).

(D) Relaxin gene signature examined for genetic vulnerability in OVCAR8 and SKOV3 cells using the CRISPR (Avana) Public 19Q4 dataset (Depmap portal).

(E) Oncoprint on ovarian serous cancer and analysis of relaxin regulated target genes indentified by RNA-seq. Data from cBioPortal.

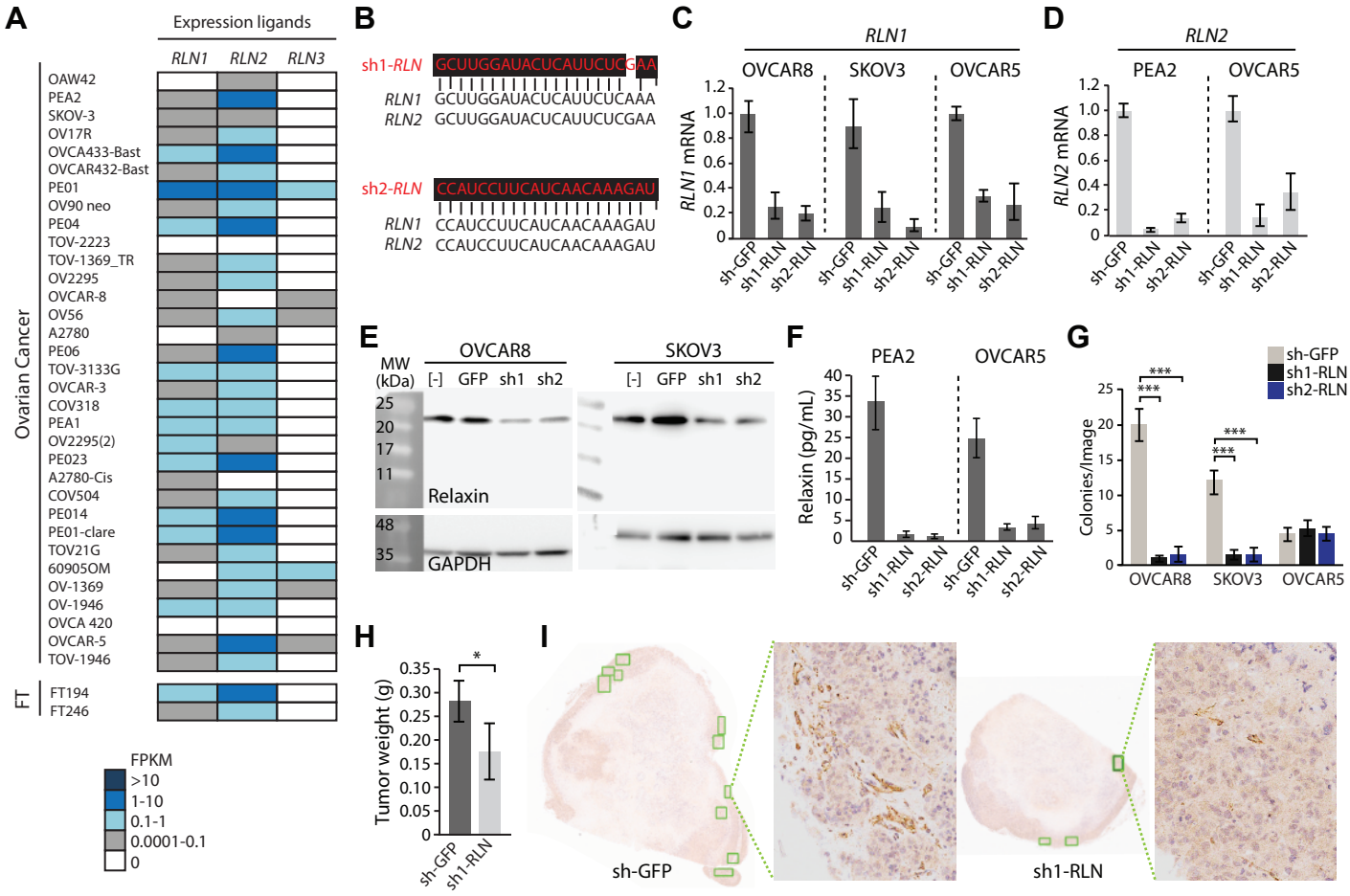

Fig.S3. Expression of relaxin in HGSOC cell lines is essential for survival. Related to Fig.3.

(A) Representation of RNAseq expression values (FPKM) for relaxin ligands in ovarian cancer and fallopian tube (FT) cell lines.

(B) Alignment of sh1-RLN and sh2-RLN target sequences to *RLN1* and *RLN2* mRNA.

(C-D) Evaluation of *RLN1* mRNA (C) and *RLN2* mRNA (D) expression following knockdown by sh1-RLN and sh2-RLN in the indicated cell lines compared to expression in sh-GFP cells.

(E) Uncropped blot showing pro-relaxin in OVCAR8 and SKOV3 parental cells [-] or cells expressing sh-GFP or shRNA targeting RLN (sh1- or sh2-) 48 hours following selection. GAPDH served as a loading control. Photograph of the molecular weight markers obtained with Microchemi-4.2 (DNR Bio-imaging Systems) software. Data represents the images cropped in Figure 3E.

(F) Relaxin levels measured by ELISA in cell culture supernatants derived from PEA2 and OVCAR5 cells expressing sh-GFP or shRNA targeting relaxin (sh1-RLN or sh2-RLN).

(G) Quantification of colonies formed in Fig.3F. Error bars indicate mean ± SEM (n=3). (***p<0.0001, Dunnett's test.).

(H) Average tumor weight (grams =g) of excised xenografts described in Figure 3G. Error bars represent mean +/- SEM. (*p<0.01, Student's t-test).

(I) IHC of CD31 staining in tumors dervied from OVCAR8 cells expressing sh-GFP control of shRNA targeting relaxin (sh1-RLN). Green boxes denote regions used for quantification based on visual detection of positive CD31 staining. The expanded regions are also shown in Fig3.

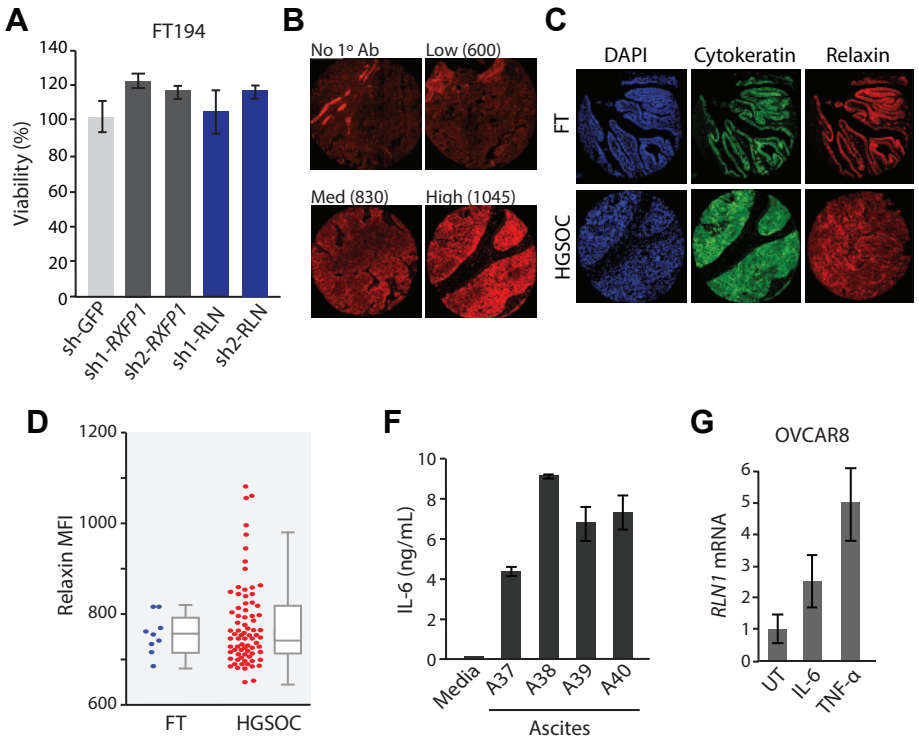

E

Parameter		Number
Number of patients (n)		48
Age (years)	Median	63
	STD	10.9412
Debulking	Primary	26
	Secondary	29
	Tertiary	1
	Interval	4
Pathology (n = 48)	High Grade Serous*	38
	Clear Cell**	3
	Other***	7
Stage	IA	2
	IIB	1
	IIIB	6
	IC	1
	IIC	2
	IIIC	31
	III	5
	IV	5
	Unknown	7
CA125		
HGSOC	Mean (μ)	827.7
	Median	222
Clear Cell	Mean (μ)	45.3
	Median	30
Other	Mean (μ)	178.9
	Median	148
Relaxin (pg/mL)		
High Grade Serous	Mean	85.3
	Median	41.9
Clear Cell	Mean	80.5
	Median	102.7
Other	Mean	114.7
	Median	53.7
Control	Mean	30.5
	Median	28.5

Fig.S4. Examination of relaxin expression in tumors and ascites. Related to Fig.4.

(A) Viability assay of FT194 cells expressing control shRNA (sh-GFP) or shRNA targeting *RXFP1* (sh1-*RXFP1*, sh2-*RXFP1*) or shRNA targeting relaxin (sh1-RLN, sh2-RLN).

(B) Validation of intensity of relaxin immunofluorescence in HGSOC tissue microarrays. Low, medium and high values estimated based on mean fluoresence intensity (MFI). Background staining indicated in the no primary antibody (No 1° Ab) panel.

(C) Immunofluorescence of relaxin expression in normal fallopian tube (FT) and HGSOC tissue microarrays. Epithelial cells are marked by cytokeratin and DAPI marks the nucleus.

(D) Quantification of Relaxin levels in normal fallopian tube and HGSOC tissue microarrays (MFI = mean floresence intensity).

(E) Table of parameters associated with patient cohort data in Figure 4. Cancer antigen 125 (CA125). Control for relaxin elisa healthy donor serum (n=14).

*High Grade Serous (Serous, Serous primary peritoneal, Serous Fallopian tube , Borderline Serous Papillary, Serous Papillary, Primary peritoneal)

**Clear Cell (Clear Cell ovarian carcinoma, High grade Clear Cell carcinoma, Clear Cell ovarian adenocarcinoma)

***Other (Granulosa cell tumor, Mixed Serous and endometroid ovarian adenocarcinoma, Pelvic mass: Polypoid Endometriosis and Fibroadipose tissue, Metastatic adenocarcinoma (BRCA1+), Mucinous adenocarcinoma of the ovary, Serous borderline, Borderline Serous with numerous psammoma bodies).

(F) IL-6 protein levels in patient derived ascites supernatant (samples A37-40) measured by ELISA.

(G) *RLN1* mRNA expression in OVCAR8 cells treated with IL-6 or TNF-α (50 μg/mL).

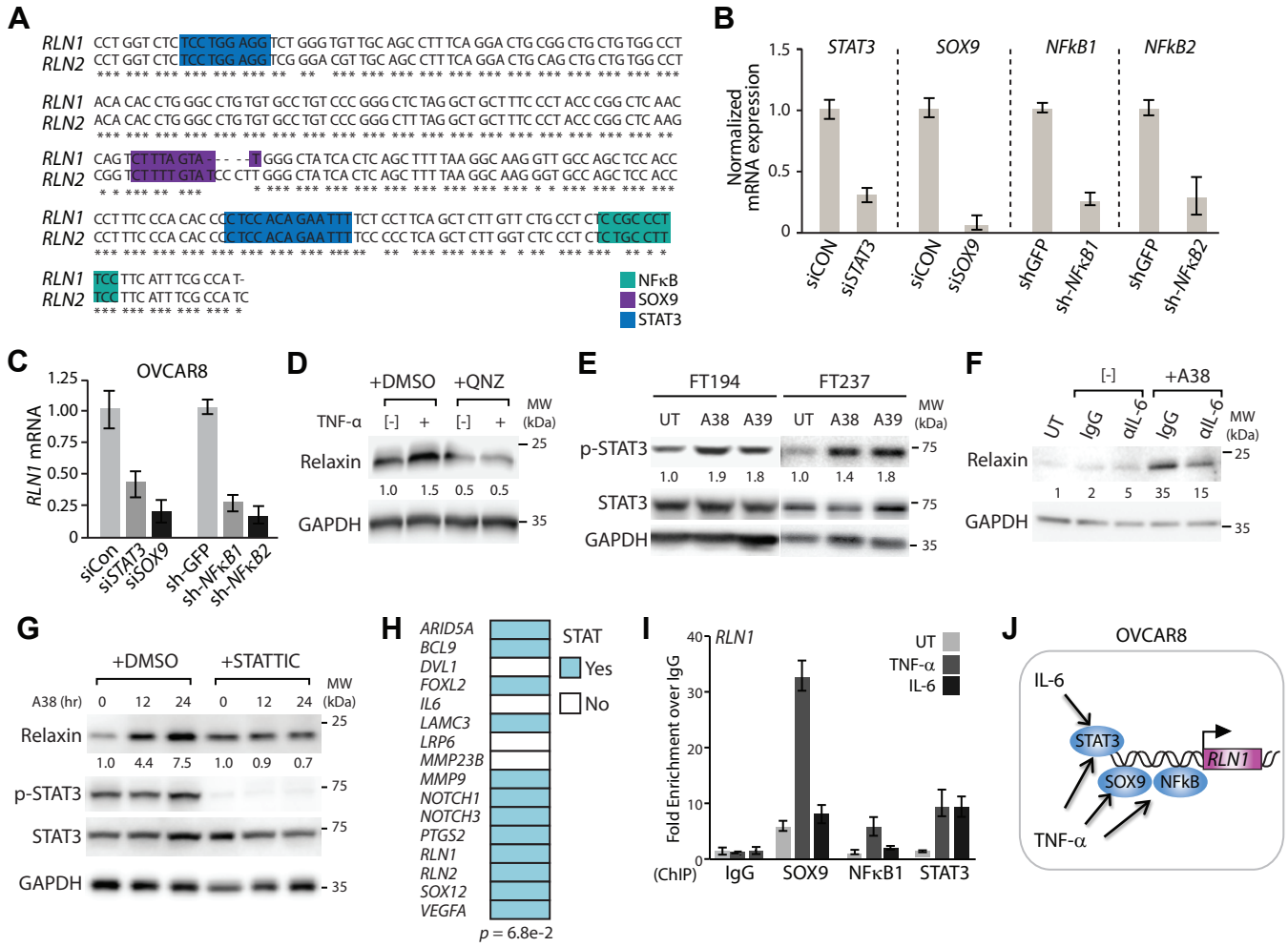

Fig.S5. Relaxin is a tanscriptional target of NFKB, STAT3 and SOX9. Related to Fig.5.

(A) Clustal alignment of *RLN1* and *RLN2* genomic regions corresponding to the proximal promoter and the minimal promoter RP-3 as reported in Fig.6. Predicted STAT3, SOX9, and NFKB binding elements defined by Transfac database are highlighted.

(B) Validation of the indicated transcription factor knockdown in OVCAR8 cells by qPCR.

(C) *RLN1* mRNA expression measured by Taqman qPCR in OVCAR8 cells transfected with nontargeting siRNA (siCon) or siRNA targeting STAT3 or SOX9 and OVCAR8 cells expressing shRNA control (sh-GFP) or shRNA targeting NFκB subunits B1 or B2.

(D) Relaxin protein levels in OVCAR8 cells treated with TNF-α (50 ng/mL) for 24 hours pre-treated with NFκB inhibitor QNZ (+QNZ) compared to cells treated with DMSO.

(E) Immunoblot of phosphorylated (p)-STAT3 (p-STAT3) in FT194 and FT237 cells 72h growth post culture in 10% ascites supernatant (a38, A39) in comparison to untreated cells (UT).

(F) Immunoblot and quantification of relaxin levels in FT-194 cells cultured in 10% ascites supernatant (+A38) compared to control treated cells (-) examined 72h post treatment. Cells were co-treated with IL-6 neutralizing antibody (αIL-6) or IgG isotype control (IgG) as indicated.

(G) Western blot of Relaxin protein levels in FT-194 cells cultured in 10% ascites supernatant (A38) for the indicated time in hours (hr) in cells pre-treated for 6 hours with STATTIC (10μM) or DMSO control.

(H) Relaxin gene signature examined for STAT binding elements in the putative promoter of the indicated genes using the motif identifed by the transfac matrix database (v7.0) annotated in human, mouse, rat alignment (DAVID and UCSC genome browser).

(I) ChIP analysis of NFκB, STAT3 and SOX9 binding on the promoter region of *RLN1* in OVCAR8 cells mock treated (UT) or treated with TNF-α (50ng/mL) or IL-6 (50ng/mL). Fold enrichment is relative to IgG.

(J) Summary of *RLN1* gene activation in OVCAR8 cells following stimulation as determined by ChIP.

A

ID #	Grade:	Stage:	Time of sampling:	Sampling Time (Months after T0):
1	4	IIIC	1st day of chemo, post surgery	T0
			End of chemo because progression	4.5
2	3	IIIC	At surgery, pre-chemo	T0
			At 2nd surgery, post-chemo	2.75
3	4	IIIC	At surgery, pre-chemo	T0
			Post-chemo, last day of treatment	4.75
4	3	IIIC	At surgery, pre-chemo	T0
			At 2nd surgery, post-chemo	4
5	3	IIIC	At surgery, pre-chemo	T0
			At 2nd surgery, post-chemo	2.25
6	4	IIIC	At surgery, pre-chemo	T0
			At 2nd surgery, post-chemo	4
7	4	II	Pre-chemo, pre-surgery	T0
			Post-chemo	4.75
8	3	IIB	At surgery, pre-chemo	T0
			At progression, 2nd surgery, post-chemo	2
9	4	IIIC	At surgery, pre-chemo	T0
			At 2nd surgery, post-chemo	2.5
10	4	IVA	At surgery, pre-chemo	T0
			At 2nd surgery, post-chemo	4.75
11	4	IIIC	At surgery, pre-chemo	T0
			At 2nd surgery, post-chemo	5.75
12	4	IIIC	At surgery, pre-chemo	T0
			At 2nd surgery, post-chemo	4.25

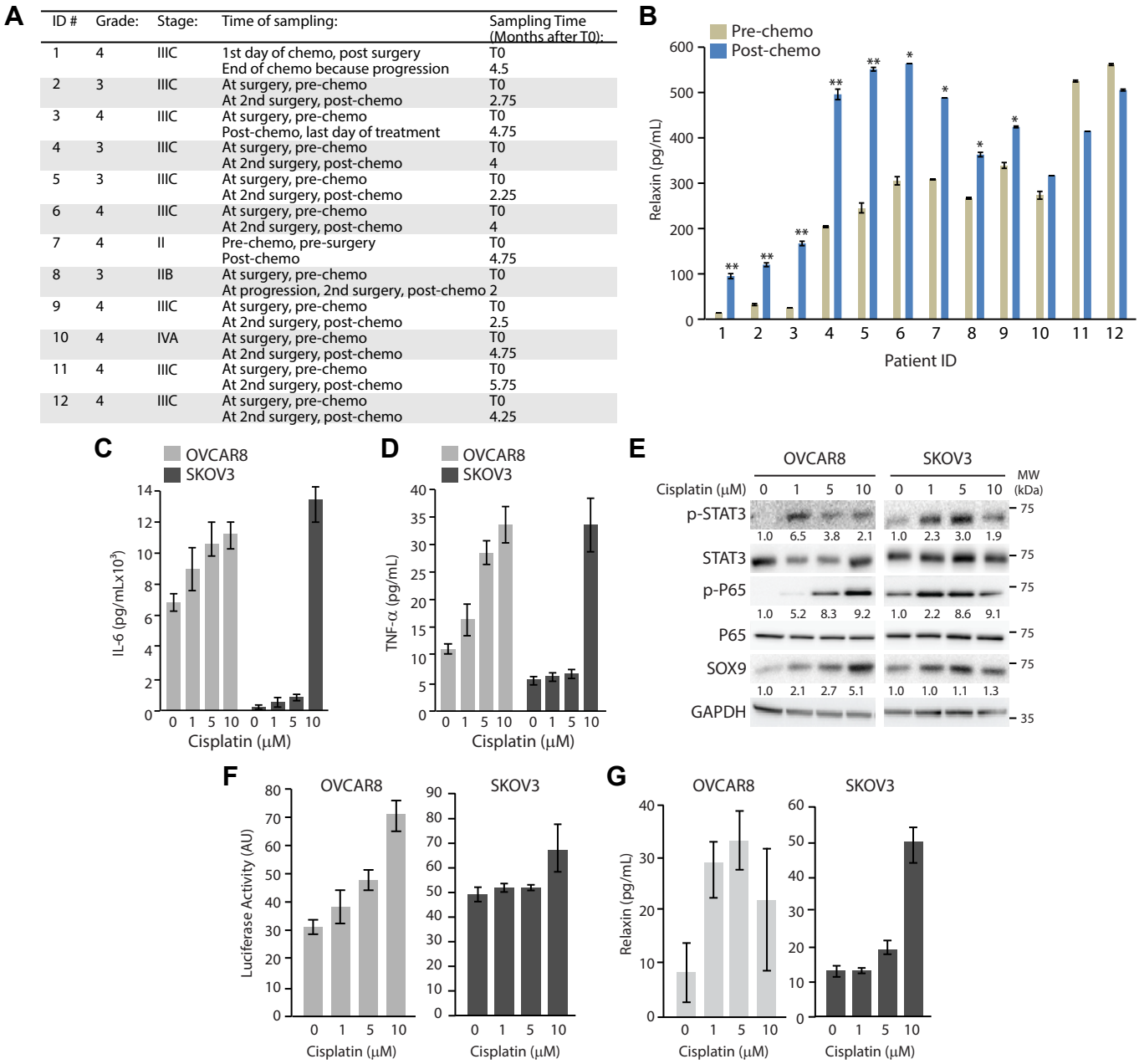

Fig.S6. Depletion of *RXFP1*-relaxin sensitizes HGSOC cells and tumors to cisplatin. Related to Fig.6.

(A) Table of patient clinical data. All patient cases are from serous cystadenocarcinoma and were treated with Taxol/Carboplatin. Time zero (T0) represents data points labeled "pre-chemo" and second sampling represent "post chemo" in panel B.

(B) Relaxin protein levels determined by ELISA in patient serum samples pre- and post-chemo. (*p<0.05 and **p<0.01, Student's t-test).

(C) IL-6 protein levels determined by ELISA in supernatants derived from OVCAR8 cells treated with increasing doses of cisplatin.

(D) TNF-α protein levels determined by ELISA in supernatants derived from OVCAR8 cells treated with increasing doses of cisplatin.

(E) Immunoblot of phosphorylated (p) STAT3 (p-STAT3), p-NFKB (p-P65) and SOX9 in OVCAR8 and SKOV3 cells following treatment with increasing doses of cisplatin.

(F) Luciferase activity (arbitrary units = AU) driven by the Relaxin promoter (RP-3) in OVCAR8 and SKOV3 cells following treatment with increasing doses of cisplatin.

(G) Relaxin protein levels determined by ELISA in supernatants derived from OVCAR8 and SKOV3 following treatment with increasing doses of cisplatin.

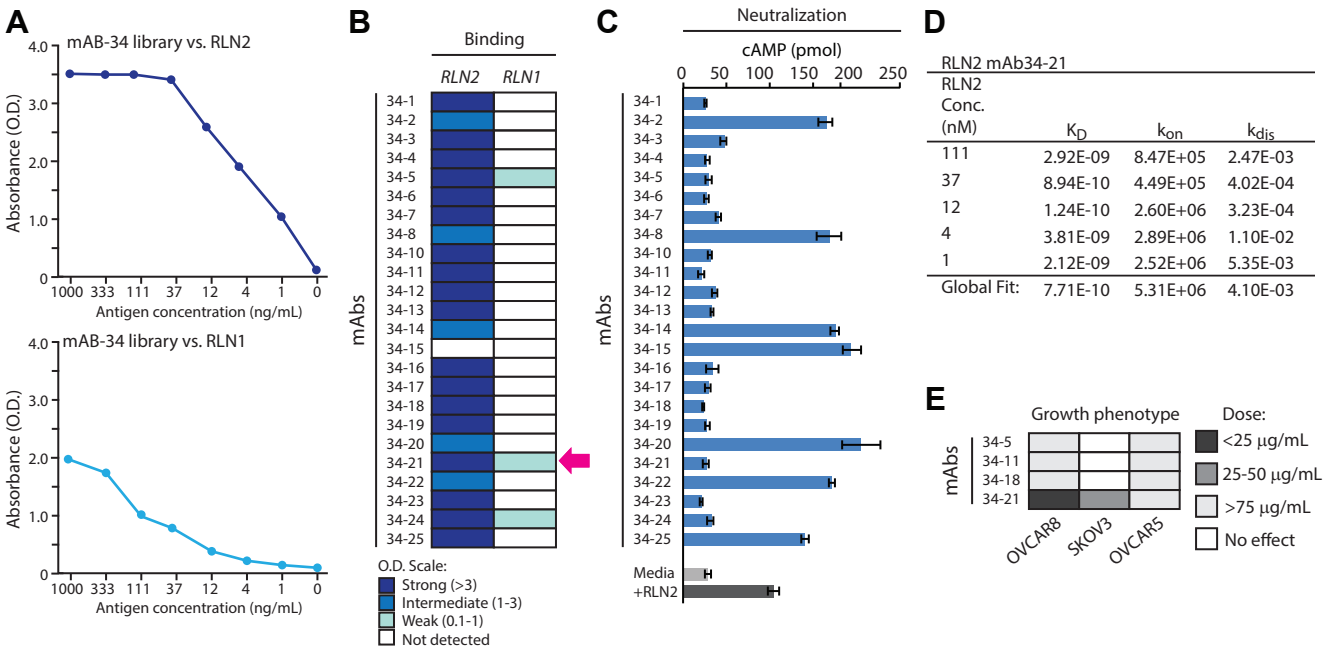

Fig.S7. Relaxin neutralizing monoclonal antibody abrogates HGSOC cell growth. Related to Fig.7.

(A) Antigen titre of hybridoma library RLN2Am34. The pooled polyclonal hybridoma library was screened for binding against serial dilutions of either RLN1 or RLN2 by ELISA.

(B) Binding analysis of anti-relaxin monoclonal antibodies (mAbs). Binding of each mAb to recombinant RLN1 and RLN2 was determined by ELISA, with colors indicating relative strength of binding to each ligand (OD value). OD values ranged from background (OD=0.05) to a maximal OD value of 3.37. Strong binding represents OD values >60X background, intermediate binding represents OD values 20-60X background OD, and weak binding represents OD values 2-20X background OD. Pink arrow highlights mAb-34-21 used in subsequent experiments.

(C) Neutralization analysis of anti-relaxin monoclonal antibodies (mAbs). Neutralizing activity represents ability to reduce cAMP accumulation in THP-1 cells by recombinant relaxin (rhRLN2). Media alone and media plus rhRLN2 (+RLN2) are indicated.

(D) Binding kinetics of purified m34-21 antibody to relaxin-2 (RLN2) at the indicated concentraions (nM = nanomolar) and assessed by Bio-Layer interferometry. Meaasure of the parameters for on rates (kon), off rates (kdis) and the overall molar affinity constant (KD) for M21 binding to each concentration of RLN2 are indicated.

(E) Ability of select anti-relaxin mAbs to reduce growth of relaxin dependent (OVCAR8 and SKOV3) and independent (OVCAR5) cells. Dose represents the minimum concentration of each mAb required to observe a growth defect.